New constraints on biological production and mixing processes in the South China Sea from triple isotope composition of dissolved oxygen

Hana Jurikova[1], Osamu Abe[2], Fuh-Kwo Shiah[3], and Mao-Chang Liang[4]

[1]School of Earth and Environmental Sciences, University of St Andrews, KY16 9TS St Andrews, United Kingdom
[2]Graduate School of Environmental Studies, Nagoya University, 464-8601 Nagoya, Japan
[3]Research Center for Environmental Changes, Academia Sinica, 11529 Taipei, Taiwan
[4]Institute of Earth Sciences, Academia Sinica, 11529 Taipei, Taiwan

Correspondence to: Hana Jurikova (hj43@st-andrews.ac.uk) and Mao-Chang Liang (mcl@gate.sinica.edu.tw)

Abstract. The South China Sea (SCS) is the world's largest marginal sea, and plays an important role in the regional biogeochemical cycling of carbon and oxygen. However, its overall metabolic balance, primary production rates, and their link to East Asian Monsoon forcing remain poorly constrained. Here, we report seasonal variations in triple oxygen isotope composition ($^{17}\Delta$) of dissolved O_2, a tracer for biological O_2, gross primary production (GP; inferred from $\delta^{17}O$ and $\delta^{18}O$ values), and net community production (NP; evaluated from oxygen–argon ratios) from the SouthEast Asian Time-series Study (SEATS) in SCS. Our results suggest rather stable mixed-layer GP rates of ~1500 mg C m^{-2} d^{-1} and NP of ~−13 mg C m^{-2} d^{-1} during the summer southwest monsoon season. These values indicate slight net heterotrophy but, within the uncertainties/variabilities observed, more likely that the metabolism of the system was in net balance. During months characterised by the relatively stronger northeast monsoon forcing, the system is more dynamic with variable production rates, which may shift the metabolism to net autotrophy (NP up to ~140 mg C m^{-2} d^{-1}). Furthermore, our data from the deeper regions show that SCS circulation is strongly affected by monsoon wind forcing, with a larger part of the water column down to at least 400 m depth fully exchanged during a winter, suggesting the $^{17}\Delta$ of deep O_2 as a valuable novel tracer for probing mixing processes. Altogether, our findings underscore the importance of monsoon intensity on shifting the carbon balance in a warm oligotrophic sea, and on driving the regional circulation pattern.

1 Introduction

The South China Sea (SCS) is the largest marginal sea of the world and significantly influences the regional biogeochemistry and climate (Wong et al. 2007a). The SCS also contributes to global circulation. A pathway through the SCS connects the tropical Pacific with Indian Ocean with impacts on the Indonesian Throughflow, a current which plays a pivotal role in the coupled ocean and climate system (Qu et al., 2005). It has been suggested that marginal seas may act as a significant global atmospheric carbon dioxide sink, primarily due to CO_2 absorption by continental shelf waters (Tsunogai et al., 1999; Liu et al., 2000; Yool and Fasham, 2001; Chen et al., 2003; Thomas et al., 2004). However, the heterogeneous nature together with

Deleted: 9AL
Deleted:),
Deleted: global as well as
Deleted: still
Deleted: trends
Deleted: 1.8 g
Deleted: −0.02 g
Deleted: , indicating the prevalence of
Deleted: .
Deleted: winter
Deleted: from net heterotrophy
Deleted: 0.15 g
Formatted: Superscript
Deleted: These findings underscore the importance of monsoon intensity on tilting the carbon balance from source to sink in a warm oligotrophic sea, and on driving the regional circulation pattern. Finally…
Deleted: conservative
Deleted: from
Deleted: new perspective
Deleted: represents
Deleted: , influencing
Deleted: as well as
Deleted: biogeochemical cycling of carbon and oxygen.
Deleted: as a whole

latitudinal differences between ocean margins makes joint extrapolations to a global scale highly uncertain. Most observations have revealed that seas at mid-latitude shelves, which experience strong spring blooms and clear seasonal patterns, function particularly well as CO_2 sinks (e.g. the North Sea (Frankignoulle and Borges, 2001); the Gulf of Biscay (Thomas et al., 2004); the Celtic Sea (Seguro et al., 2019); the East China Sea (Tsunogai et al., 1999; Wang et al., 2000) or the Middle Atlantic Bight (DeGrandpre et al., 2002)). Conversely, the tropical and subtropical shelves and marginal seas, on the other hand, are most likely CO_2 sources due to their high annual surface temperatures and the absence of strong spring blooms (Cai and Dai, 2004). A similar scenario may also be anticipated for the SCS. While several studies reaffirmed that the SCS indeed acts as a source of CO_2 to the atmosphere in the spring, summer and autumn (Rehder and Suess, 2001; Zhai et al., 2005), Tseng et al. (2005) reported on the uptake of CO_2 during winter from the SCS. The observed CO_2 invasion, driven by an unusual seasonal pattern in the oligotrophic open northern part of the SCS with elevated chlorophyll concentrations (0.3–0.35 mg m^{-3}) and primary production (300 mg C m^{-2} d^{-1}), was apparently large enough to compensate for the CO_2 evasion during the rest of the year, resulting in only minor net annual sea–atmosphere CO_2 fluxes (0.24 g C m^{-2} yr^{-1}; Tseng et al., 2007). Although the primary production and phytoplankton biomass are low for most of the year in the SCS, it appears that a clear winter maximum can be found regularly; a distinct seasonal pattern from other low latitude waters bodies. Clearly, the role of the SCS, and marginal seas in general, is complex and their seasonal carbon cycling and demands further study.

Owing to its geographical position between the Tibetan Plateau and the western Pacific warm pool, the SCS is continuously exposed to the East Asian Monsoon, which plays a fundamental role in its the oceanography and biogeochemistry (see Wong et al., 2007a for an overview). From June to September, the weaker southwest summer monsoon (SWM) drives the anti-cyclonic circulation gyre, while the strong northeast winter monsoon (NEM) propels a basin-wide cyclonic circulation gyre between November and April (Fig. 1). This intense seasonal reversal drives the short- and long-term physical, chemical and biological processes that control the distribution of phytoplankton communities (Ning et al., 2004). As a result, intermediate chlorophyll a (Chl−a) concentrations are typically associated with the SWM, while the highest phytoplankton biomass is expected during the NEM due to increased diapycnal nutrient supply from the thermocline. Winter mean Chl−a concentrations often peak at about 0.5 mg m^{-3} in the subsurface chlorophyll maximum and at 0.2 mg m^{-3} at the surface (Liu et al., 2002). Upwelling produced by the convergence of currents in the cyclonic gyre near the Luzon Strait where the Kuroshio intrudes, can at times enhance the mean Chl−a concentration (about 0.65 mg m^{-3}) and primary production in winter to about 8 times the summer values (Chen et al., 2006). Conversely, lowest Chl−a values have been observed during inter-monsoon seasons (Liu et al., 2002; Wong et al., 2007b; Li et al., 2017). Superimposed on the main seasonal monsoon-driven pattern, episodic events such as typhoons may temporarily elevate primary production due to wind-enhanced vertical mixing, bringing nutrients from the nutricline to the mixed layer and stimulating production. For instance, Lin et al. (2003) reported a bloom patch with average surface Chl-a concentrations of 3.2 ± 4.4 mg m^{-3} during the passing of a tropical cyclone Kai-Tak in July 2000. In addition to typhoons, the SCS has been suggested to be sensitive to various types of short-term physical forcings including tides, internal waves, eddies or topography-flow interactions. Generally, these tend to enhance vertical mixing, supplying nutrient-rich waters

Deleted: any
Deleted: unrepresentative.
Deleted: observation
Deleted: , in particular
Deleted: The
Deleted: ,
Deleted: the
Deleted: temperature
Deleted: Similar
Deleted: phytoplankton biomass in
Deleted: during winter,
Deleted: Tseng et al., 2005).
Deleted: needs to be further examined. This presents an even more pressing challenge under the current on-going climatic changes, and will be critical for improving our future CO_2 projections and climate models…
Deleted: of the SCS
Deleted: 2007
Deleted: ;
Deleted: between November and April
Deleted: patterns
Deleted: medium
Deleted: productivity
Moved down [1]: ; Li et al., 2017).
Deleted: Lowest Chl−a
Moved (insertion) [1]
Deleted: 2007).

to the mixing layer, which enhance phytoplankton production and Chl-a concentration (to about 0.3–0.4 mg m^{-3}) in the oligotrophic waters of the SCS. Interannual variability in the SCS is primarily driven by the ENSO (El Niño–Southern Oscillation), which modulates the strength of the monsoon forcing, which in turn affects the regional marine biogeochemistry. During warm (cold) El Niño (La Niña) episodes in the Pacific, the monsoon tends to have a late (early) onset and the monsoon intensity is generally weaker (stronger; Zhou and Chan, 2007). Consequently, weakened wind mixing and strengthened water column stratification results in anomalously low Chl-a concentrations in the northern SCS. For example, the 1997–1998 El Niño event was one of the most powerful ENSO events in recorded history and caused concentration of surface Chl-a to drop from 0.2 to 0.1 mg m^{-3} in the northern SCS and the mean winter production to be reduced by about 40% (Shang et al., 2005; Tseng et al., 2009).

Accurate quantification of phytoplankton production rates, a fundamental property of the ocean system, remains a challenge, primarily due to methodological biases. This has been a subject of increasing debate over the past years resulting in augmented efforts to compare and resolve production rates through different methods (e.g. Juranek and Quay, 2013; Regaudie-de-Gioux et al., 2014). In the SCS and at the SouthEast Asian Time-series Study (SEATS; Wong et al., 2007a) our understanding of primary production is predominantly limited to opportunistic assessments using the ^{14}C-assimilation method (Liu et al., 2002) or satellite-based SeaWiFS observations (Liu et al., 2002; Lin et al., 2003). While the traditional ^{14}C approach (Steeman-Nielsen, 1952) is limited due to its in vitro nature, which cannot reflect the time-averaged mixed-layer phytoplankton production (Marra, 2002), the latter relies on calibrations against field measurements that are spatially and temporally scarce (Carr et al., 2006). Although not exempt of uncertainties (Juranek and Quay, 2013), as these are inherent to any productivity determination, the triple oxygen isotope composition ($^{17}\Delta$) technique (Luz et al., 1999; Luz and Barkan, 2000) combined with O_2/Ar measurements has proved to be a powerful tool to provide a new perspective on evaluating primary production (e.g. Sarma et al., 2005; Reuer et al., 2007; Stanley et al., 2010; Hamme et al., 2012; Castro-Morales et al., 2013; Jurikova et al., 2016). The key advantage of this technique is that $^{17}\Delta$ allows for distinguishing photosynthetic O_2 input from other sources directly in situ, while the co-variation of $\delta^{17}O$ and $\delta^{18}O$, the dual-delta approach (Prokopenko et al., 2011; Kaiser, 2011), enables an estimation of the integrated gross productivity in the mixed layer.

In order to evaluate the photosynthetic O_2 production and its contribution to the local carbon balance, as well as improve our understanding of seasonal variabilities in primary production in the SCS, we performed triple isotopic analyses and determined the O_2/Ar of dissolved O_2 samples from five vertical profiles during the occupation of SEATS in October 2013, August 2014 and April 2015. We combine the $^{17}\Delta$ and O_2/Ar tracers to study the seasonal trends in photosynthetic vs. atmospheric O_2 input in the upper water column (~200 m), which we relate to the main monsoon seasons. Gross and net primary production rates are also estimated and discussed. Finally, owing to the limited contribution from photosynthesis and air-sea gas exchange to $^{17}\Delta$ signal in a parcel of deep water (200 to 3500 m), the potential for the application of the tracer for assessing mixing processes is discussed.

Deleted: however,
Deleted: , principally
Deleted: Alone in
Deleted: later
Deleted: $^{17}\Delta$;
Deleted: providing us
Deleted: a more exact assessment
Formatted: Subscript
Deleted: ,
Deleted: , and expand
Deleted: overall
Deleted: and its link to monsoon forcing
Deleted: ($^{17}\Delta$)
Deleted: seasonal
Deleted: at
Deleted: . The profiles represent summer SMW
Deleted: winter NEM as well as inter-monsoon conditions. In addition…
Deleted: conservative behaviour of $^{17}\Delta$
Deleted: , we use the deep samples to further review
Deleted: this
Deleted: from a new perspective

2 Methods

2.1 Sampling and analysis

Sampling was carried out aboard R/V OR-1 during cruises CR1053 (in October 2013), CR1084 (August 2014) and CR1103 (April 2015) at station 55 "SEATS" (the SouthEast Asian Time-series Study, 18° N, 116° E, Fig. 1) in the South China Sea (SCS). Seawater was collected using a rosette sampler equipped with 20-L Niskin bottles attached to a Seabird SBE 911 Plus CTD. Samples for dissolved oxygen analysis were obtained on October 16th in 2013 (11 depths: 5, 10, 30, 50, 80, 100, 150, 200, 300, 400 and 500 m), on August 5th (11 depths: 5, 10, 20, 80, 100, 200, 600, 1000, 1800, 2500 and 3500 m) and 6th in 2014 (13 depths: 5, 10, 20, 50, 80, 200, 400, 600, 1000, 1200, 1800, 2500 and 3500 m), and on April 24th (14 depths: 5, 10, 20, 80, 100, 150, 200, 300, 400, 500, 600, 1000, 1800 and 3500 m) and April 25th in 2015 (7 depths: 5, 10, 20, 30, 50, 80, 100; see also Supplement).

The accuracy of dissolved oxygen concentration measurements from the CTD was verified and calibrated against in vitro measurements. Briefly, water samples were siphoned into triplicate 60 ml bottles (Wheaton) and the Winkler titration method of Pai et al. (1993) was adopted for in vitro dissolved O_2 determination with a precision of 0.2 % r.s.d. (full scale). Concentrations of Chl–a were measured by a fluorometer (Chelsea AQUA tracka III) attached to the CTD to monitor vertical profiles of fluorescence, which was calibrated by in situ Chl–a measurements by a Turner Designs fluorometer (10-AU-005) after extraction with 90% acetone using a non-acidification method (Gong et al., 1996). The precision of Chl–a measurements using a Turner fluorometer is usually better than 8 % for any chlorophyll values exceeding 0.5 mg m^{-3} (Strickland and Parsons, 1972), with any uncertainties on the estimation of Chl–a linked to the presence of Chl–b being below 5 %. (Lorenzen, 1981). We compared two mixed layer depth definitions; (1) temperature-based definition defined by 1 °C (ΔT) threshold from reference temperature value at 10 m depth, and (2) dissolved O_2-based definition defined by 1 % (ΔO_2) threshold from reference O_2 concentration at 10 m depth. Selected mixed layer depths were further verified by careful visual of vertical temperature, density and dissolved oxygen profiles. The limit of the photic zone was defined as the depth where the photosynthetically active radiation (PAR) was 1 % of the surface value. We used Ocean Data View (ODV; Schlitzer, 2020) for profile visualisation.

Triple oxygen isotope analyses were carried out at Academia Sinica, Taiwan. The triple oxygen isotope composition, or ^{17}O-excess (Luz et al., 1999; Luz and Barkan, 2000) is defined as:

$$^{17}\Delta = [\ln(1+\delta^{17}O) - \lambda \times \ln(1+\delta^{18}O)], \quad (1)$$

where the isotopic compositions $\delta^{17}O$ and $\delta^{18}O$ represent the deviation of the abundance ratio of an isotopic and normal species in a sample relative to that of a standard:

Deleted: Mixed

Deleted: was

Deleted: inspection

Deleted: Limit

Moved down [2]: The laboratory protocols for dissolved oxygen sample preparation and analysis are detailed in Jurikova et al. (2016).

Deleted: For comparison, selected sample duplicates obtained from the cruise in October 2013 were also measured at Nagoya University, Japan following the protocols previously described in Sarma et al. (2005). …

Moved down [3]: Note that O_2–Ar data is not available for the October 2013 profile due to the setting of gas chromatograph condition at dry ice-acetone slush temperature for complete separation of O_2.

Deleted: ¶
¶

Moved down [4]: In summary, dissolved gases were extracted from water following Emerson et al. (1995) and Luz et al. (2002).

Deleted: $\delta^{17}O$ and $\delta^{18}O$ in O_2 from the purified oxygen-argon mixture were determined by dual inlet mass spectrometry (Thermo Scientific Finnigan MAT 253 IRMS).

Formatted: Font colour: Auto

$$\delta^{*}O = \left[\left({}^{*}O/{}^{16}O\right)_{sample}/\left({}^{*}O/{}^{16}O\right)_{standard} - 1\right], \quad (2)$$

where $^{*}O$ is either ^{17}O or ^{18}O. Here, $\delta^{17}O$ and $\delta^{18}O$ are expressed with respect to atmospheric air O_2, and following Luz and Barkan (2005) the factor λ is taken to be 0.518. As suggested by Luz and Barkan (2011), we note that a slope of $\lambda = 0.516$ might present a more appropriate choice. However, in order to enable a direct comparison to other studies, we prefer the earlier value, which has been largely applied in studies on marine production. The use of a slope $\lambda = 0.516$ would result in only a minor increase in $^{17}\Delta$ (about 1–8 % of the reported values), which for most of our samples remains within analytical uncertainties.

The laboratory protocols for dissolved oxygen sample preparation and analysis are detailed in Jurikova et al. (2016). Note that O_2–Ar data is not available for the October 2013 profile due to the setting of gas chromatograph condition at dry ice-acetone slush temperature for complete separation of O_2. In summary, dissolved gases were extracted from water following Emerson et al. (1995) and Luz et al. (2002). $\delta^{17}O$ and $\delta^{18}O$ in O_2 from the purified oxygen-argon mixture (or pure oxygen for October 2013 samples) were determined by dual inlet mass spectrometry (Thermo Scientific Finnigan MAT 253 IRMS). Similar as in Jurikova et al. (2016) an Ar correction was performed to correct for the distribution of gases between the headspace and water in the sampling flasks and normalised to air. A size correction for the total amount of gas in the sample was not required at our current mass spectrometer setting and hence not applied. Our actual and long-term precision (1σ, standard deviation) established from routine measurements (n = 36) of atmospheric air O_2 for $\delta^{17}O$, $\delta^{18}O$, and $^{17}\Delta$ is 0.017 ‰, 0.030 ‰, and 6 per meg, respectively, and our O_2 scale (Jurikova et al., 2016; Liang and Mahata, 2015; Liang et al., 2017) is in agreement with that of Luz and Barkan (2011). The O_2/Ar ratio was obtained by peak jumping following Barkan and Luz (2003), and is expressed as $\delta(O_2/Ar)$ (‰) = $[(32/40)_{sample}/(32/40)_{standard} - 1] \times 10^3$. The long-term precision (1σ) of routine measurements of atmospheric air was better than 5 ‰. The reproducibility (1σ) for the analysis of equilibrated water samples (n = 3) was 0.020 ‰, 0.037 ‰, and 11 ± 3 per meg for $\delta^{17}O$, $\delta^{18}O$, and $^{17}\Delta$, respectively and 4.6 ‰ for $\delta(O_2/Ar)$; see Jurikova et al. (2016) for further details.

2.2 Primary production calculations

To quantify gross production rates from $\delta^{17}O$ and $\delta^{18}O$ values we followed the standard "dual-delta approach" following Prokopenko et al. (2011) and Kaiser (2011), where the gross oxygen production may be calculated as follows:

$$GOP = KC_o \left[\frac{\left(1-\frac{1+\delta^{17}O_{eq}}{1+\delta^{17}O}\right) - 0.518\left(1-\frac{1+\delta^{18}O_{eq}}{1+\delta^{18}O}\right)}{\left(\frac{1+\delta^{17}O_p}{1+\delta^{17}O}-1\right) - 0.518\left(\frac{1+\delta^{18}O_p}{1+\delta^{18}O}-1\right)}\right], \quad (3)$$

Deleted: We note that as
Deleted:)
Deleted: , however
Deleted: only
Deleted: the
Deleted: the
Moved (insertion) [2]
Moved (insertion) [3]
Moved (insertion) [4]
Deleted: c

where δ^*O is the measured value in a sample, δ^*O_{eq} is the air-water equilibrium (Jurikova et al., 2016), and δ^*O_p represents the photosynthetic O_2 (Luz and Barkan, 2011). C_o is the O_2 concentration at saturation using solubility coefficients from Benson and Krause (1984) and K is the piston velocity, the coefficient for gas exchange. K was calculated using the quadratic relationship appropriate for wind speeds between 3 and 15 m s^{-1} ($K = 0.24 \times U^2_{10} \times (Sc/660)^{-0.5}$) and normalised to Schmidt number 666 (Sc_{660}) based on mixed layer temperatures (Wanninkhof et al., 2009). We compared two different approaches for deriving K, and the resulting K values are available in Table 1. First, we used a simple approach where K was derived from mean NCEP wind speeds (Fig. 2) and averaged over the O_2 residence time in the mixed-layer preceding sampling (K_{avg}; 16, 7, and 4 days for October 2013, August 2014 and April 2015, respectively), based on the mixed-layer depth and the gas transfer coefficient. Second, we used the approach of Reuer et al. (2007) where K was calculated using a weighting technique, which considers variable wind speeds and accounts for the fraction of mixed layer ventilated each day (K_{wgh}). For this, K was derived from satellite wind speed measurements of hourly resolution using the ERA5 dataset (ECMWF, European Centre for Medium-Range Weather Forecasts, https://www.ecmwf.int/). Following Reuer et al. (2007), the fraction of the mixed layer ventilated on the collection date (f_1) was determined from the mixed layer depth (Z_{MLD}) and gas transfer velocity on the collection day (K_1) as $f_1 = K_1 \times 1day/Z_{MLD}$, and was assigned a weight $\omega_1 = 1$. The fraction of the mixed layer ventilated prior to the sample collection day (day 2) was similarly calculated as $f_2 = K_2 \times 1day/Z_{MLD}$, but was assigned a reduced weight according to the fraction of the mixed layer ventilated on day 1 ($\omega_2 = \omega_1 \times (1–f_1)$). Since the SEATS station was occupied for a limited time only during each cruise, we used the Z_{MLD} of the collection date for all calculations. Considering the rather regular interannual pattern and minimal daily variations in the mixed layer depth, the used mean value should be a suitable representation for the different sampling months (see also Section 3.1). The weight on the t^{th} day prior to the sampling is described by the general term $\omega_t = \omega_{1-1} \times (1– f_1)$. A weighted gas transfer velocity for each day was then calculated as $k_t\omega_t$, and the weighted gas exchange rate for the mixed layer as:

$$k = \frac{\Sigma_{t=1}^{30} k_t \omega_t}{(1-\omega_{30})\Sigma_{t=1}^{60} \omega_t} \quad (4)$$

where the term $(1 – \omega_{30})$ accounts for the residual unventilated portion of the mixed layer. We utilised 30 days for each sampling date (October 2013, August 2014 and April 2015) as the residual fraction on the 30th day was already minimal. The two approaches for deriving K resulted in different production rates, with the K_{avg} either underestimating or overestimating production when compared to K_{wgh}, by ~38 % in October 2013, ~47 % in August 2014, and ~21 % in April 2015 for both GP and NP (since the choice of K affects GP and NP proportionally). We therefore used K_{wgh} values for calculating the NP and GP rates at SEATS.

Mixed-layer O_2 production time (O_2 concentration in the mixed layer / O_2 gross production rate) was determined to evaluate the rate at which O_2 was produced biologically against the physical O_2 residence time. The O_2 production time was estimated

Formatted: Subscript

Deleted: wind speeds measured on the ship using an anemometer and verified against

Deleted: data (Fig. 2). Considering the high

Deleted: in SCS during the cruises, K was calculated following Ho et al. (2006),

Deleted: Mixed-layer O_2 production time

Deleted: estimated from measured O_2 concentrations and GOP data, and was generally lower than O_2 residence time (0.5 days for October 2013, 1.5

Deleted: 1.0 days for April 5th

Deleted: 6th 2014, respectively

Deleted: 0

Deleted: 3.6 days for April 24th

Deleted: 25th 2015, respectively).

from the measured O_2 concentrations and the GOP and was generally lower than O_2 residence time (0.5 days for October 2013, 1.5 and 1.0 days for April 5th and 6th 2014, respectively, and 1.0 and 3.6 days for April 24th and 25th 2015, respectively).

To assess the net production rates (NOP), we used the O_2/Ar measurements consistent with the biological O_2 supersaturation concept for net photosynthetic production. Because the physical properties of O_2 and Ar are similar, and Ar has no biological sources and sinks, measurements of Ar concentration in water may be used to remove physical contributions to O_2 supersaturation. The biological oxygen supersaturation $\Delta(O_2/Ar)$ is defined as the relative deviation of the O_2/Ar in a sample to the O_2/Ar at equilibrium (given in %) with the atmosphere (e.g. Craig and Hayward, 1987; Emerson et al., 1995; Kaiser et al., 2005) and may be calculated as follows:

$$\Delta(O_2/Ar) = \left[\frac{1+\delta(O_2/Ar)_{sample}}{1+\delta(O_2/Ar)_{eq}} - 1\right], \quad (4)$$

NOP can be calculated from $\Delta(O_2/Ar)$ values following Luz et al. (2002):

$$NOP = K \times C_o \times [\Delta(O_2/Ar)]. \quad (5)$$

It is important to note here that the estimation of both GOP and NOP via the presented approaches relies on the assumption that the mixed layer is at a steady state, and that there is no significant entrainment or upwelling of low-O_2 subsurface water into the mixed layer, nor lateral advection from adjacent waters. Production rates were converted from O_2 to C units following a commonly applied approach (e.g., Hendricks et al., 2014; Juranek et al., 2012). To scale GOP to gross C production, we account for the fraction of O_2 linked to Mehler reaction and photorespiration following Laws et al. (2000) by applying a photosynthetic quotient (PQ) of 1.2. For NOP conversion we use a PQ of 1.4 for new production (Laws, 1991). Hereinafter, we refer to the scaled production rates as GP and NP.

3 Results

3.1 Oceanographic setting

Vertical distribution of physical parameters, chlorophyll and dissolved O_2 composition were measured from profiles collected during October 2013, August 2014 and April 2015. Generally, during the sampling for this study the mixed layer temperature variations were only minor and varied depending on the month. Highest surface temperatures of 29 °C were recorded during the summer in August 2014. In October 2013, the average temperature was 28 °C and the lowest values of 27 °C were observed in April 2015. Temperature-based mixed layer depth limit was deepest on the 16th of October 2013 at 49 m. In August 2014, the mixed layer was relatively shallow, but changed from 5th to 6th August from 25 m to 34 m. In April 2015, the mixed layer

Deleted:)
Deleted: have
Deleted: , following
Deleted: Assuming the mixed layer is at steady state,
Deleted: the standard
Deleted: comparing to the low-latitude Hawaii Ocean Time-series (HOT)
Moved down [5]: station (Karl et al., 1996), the SEATS station located at an even lower latitude is characterised by a distinct phytoplankton biomass and primary production pattern (Tseng et al.,
Moved down [6]: 2005; Wong et al.,
Deleted: In contrast to the typical features
Deleted: tropical waters, characterized by minimal seasonal variations,
Deleted: 2007), largely governed by the East Asian Monsoon which plays a key role in the oceanography and biogeochemistry of the SCS (Chao et al., 1996a; Liu et al., 2002). To assess the role of the monsoon forcing on biological production we
Deleted: samples
Deleted: the typical monsoon seasons: the inter-monsoon period in
Deleted: the summer southwest monsoon (SWM) in April 2014, and the winter northeast monsoon (NEM) in
Deleted: The basin-wide prevailing monsoon forcing coinciding with our sampling period is also evident from the surface wind maps (Fig. 2). ¶
¶
Shallow mixed layer and persistent stratification throughout the year are characteristic features of SEATS. Overall,
Deleted: depended
Deleted: (Fig. 3).
Deleted: in
Deleted: (Fig.
Moved down [7]: 3b).
Deleted: (Fig. 3a)
Deleted: ,
Deleted: towards the end of the winter monsoon
Deleted: (Fig.
Moved down [8]: 3c).
Deleted: Conversely,
Deleted: in
Deleted: In August 2014

depth was 28 m and 26 m on the 24th and 25th, respectively (Table 1). In addition to the temperature-based criterion, we considered the dissolved O_2 mixed layer definition of Castro-Morales and Kaiser (2012) based on a relative difference of 0.5 % in O_2 concentration to a reference value at 10 m. We, however, did not find the 0.5 % definition suitable, as the oscillations in the O_2 concentrations in mixed layer alone were on the order of 0.5%. Instead, we used a threshold of 1 % which also closely agreed with the visual inspection of the profiles. This definition resulted in a mixed layer depth of 48 m on the 16th of October 2013, 20 m and 32 m on the 5th and 6th August 2014, and 27 m and 25 m on the 24th and 25th April 2015, respectively (Table 1). The mixed layer depths determined by the different criteria were in close agreement within 2 m, except for 5th August 2014 when the difference between the definitions was 5 m. As the O_2-based definition is more conservative and directly related to the species of interest of this study, we used the O_2-based mixed layer depths for estimating integrated mixed layer production from dissolved O_2.

The observed mixed layer depths and interannual pattern fit well within the trend expected for SEATS, which appears to stays rather regular between years (Wong et al., 2007; Tai et al., 2017). A shallow mixed layer (about 20 m deep in summer and up to 100 m in winter) and a persistent stratification throughout the year are characteristic features of SEATS. The average maximum mixed layer depth at SEATS is ~80 m occurring in December and January. Throughout spring, the mixed layer depth steadily decreases reaching minimum ~25 m in May. The mixed layer increases again gradually reaching ~35 in June and remains approximately constant through to October, after which it increases sharply to reach its maximum winter values (Tai et al., 2017).

The chlorophyll fluorescence was generally low and restricted to the thermocline in the upper 50−100 m (Fig. 3), as expected for the oligotrophic northern SCS (see Section 1), with the absolute magnitude of the subsurface maximum peak varying between seasons. Interestingly, Chl−a was highest of 0.6 mg m^{-3} in October 2013 (Fig. 3a). In August 2014 the concentration remained at 0.2−0.3 mg m^{-3} without pronounced variations and diurnal trends (Fig. 3b). In April 2015 we observed again a minor increase in the subsurface chlorophyll maximum, but mostly restricted to the dawn hours of up to 0.5 mg m^{-3}, which gradually declined throughout the day and was lowest at night of approximately 0.2 mg m^{-3} (Fig. 3c).

The dissolved O_2 saturation in the upper 400 m on the different sampling days is shown in Figure 3d. In October 2013, the mixed layer was saturated between 100 % and 102 % and below, in the thermocline, O_2 saturation decreased. In August 2014, the O_2 was saturated throughout the mixed layer (100 %) on the first collection day, and between 97–98 % on the second day. In April 2015, the mixed layer O_2 saturation hovered between 97–98 % on the first day, and 102–103 % on the second day. Below the limit of the mixed layer O_2 saturation increased by few % in August 2014 as well as on 24th April 2015. A more prominent supersaturated O_2 peak reaching 110 % below the mixed layer was observed on April 25th 2015.

Deleted: was situated at 31 m and the shallowest mixed layer of 23 m…

Deleted: recorded in April 2015

Deleted: , Fig. 3).

Deleted: Chlorophyll

Deleted: depths (Fig. 4). Nevertheless, we observed relatively marked seasonal variations.

Deleted: during the inter-monsoon period

Deleted: 4a

Deleted: , during the summer SWM,

Moved (insertion) [7]

Moved down [9]: 4b).

Deleted: For the winter NEM season

Deleted: (April 25th, 2015),

Moved (insertion) [8]

Based on our sampling months and the observed physical parameters the profile from October 2013 appears to reflect the transition from summer to winter conditions. The lack of basin-wide prevailing monsoon forcing is also evident from surface wind maps (Fig. 2a), indicating that this collection date might largely represents an inter-monsoon period. The shallow mixed layer in August 2014 and southwest wind direction point towards typical summer monsoon conditions (Fig. 2b). Conversely, the mixed layer characteristics in April 2015 are suggestive of spring conditions, although the surface wind maps still indicate the presence of the northeast winter monsoon in the area (Fig. 2c). We therefore conclude that the April 2015 collection days likely reflect late northeast (winter) monsoon season during spring.

3.2 Dissolved O_2 composition: $^{17}\Delta$ and $\Delta(O_2/Ar)$

The triple isotope composition of dissolved O_2 profiles from SEATS is shown in Figure 4. We observed broad seasonal variations in both the $^{17}\Delta$ and the $\Delta(O_2/Ar)$, with a daily component, overall ranging between 22 and 229 per meg and −72 to 2.2 %, respectively. At large, the upper $^{17}\Delta$ profiles outlined a common trend, with low $^{17}\Delta$ in the mixed layer, a peak in the values below, and a gradual decrease towards 200 m depth. The average mixed layer values (Table 1), and the depth of the $^{17}\Delta$ maximum peak as well as its magnitude, however, varied considerably between the months and collection days. Highest mixed layer $^{17}\Delta$ values averaging 90 ± 28 were observed in October 2013. On August 5th and 6th 2014 and April 24th 2015 the O_2 composition were comparable yielding $^{17}\Delta$ values of 59 ± 9, 54 ± 18 and 52 ± 11, and $\Delta(O_2/Ar)$ values of –0.3 ± 0.5, –0.2 ± 0.2, and –0.5 ± 3.5, respectively.

Largest variations in $^{17}\Delta$ and $\Delta(O_2/Ar)$ were observed in the thermocline. In October 2013, the $^{17}\Delta$ gradually increased with depth to a maximum of 182 per meg at 80 m, and then decreased (Fig. 4a). In August 2015, the highest $^{17}\Delta$ values reached 218 per meg at 100 m measured on the 5th (Fig. 4b). The depth trend on the 6th fairly resembled the one from the 5th, but the $^{17}\Delta$ values between the two days varied up to 61 per meg at 150 m. In April 2015, the $^{17}\Delta$ variations were comparatively subtle, without a prominent sharp peak, ranging between 140 and 125 per meg in the upper 50 m to 150 m. A deep peak in $^{17}\Delta$ was observed at 600 m of 223 per meg (Fig. 4c).

4 Discussion

4.1 Seasonal trends in photosynthetic vs. atmospheric O_2 input in the upper water column

The combined approach of $^{17}\Delta$ and $\Delta(O_2/Ar)$ composition of dissolved O_2 has been shown to be a valuable tracer for distinguishing biologically mediated O_2 from that supplied by atmospheric air input to the euphotic zone (Luz et al., 1999; Luz and Barkan, 2000). This is because atmospheric O_2 has a unique isotopic signature generated by stratospheric photochemical reactions involving O_3, O_2, and CO_2 which fractionate its isotopes in a mass-independent way (e.g. see Lämmerzahl et al., 2002), while photosynthesis fractionates O_2 isotopes in a mass-dependant way. By definition, the atmospheric $^{17}\Delta_{atm} = 0$, although the air-water equilibrium $^{17}\Delta_{eq}$ deviates slightly from the atmospheric value ($^{17}\Delta_{eq} = 11 \pm 3$ per meg, see Section 2.1;

Moved down [10]: 4c).

Deleted: 3 and available in Supplement.

Deleted: ,

Deleted: seasons. In the shallow mixed layer in August 2014 (Fig. 3b) and April 2015 (Fig. 3c), the $^{17}\Delta$ ranged between ~20−70 per meg due to the fast-changing balance between O_2 produced photosynthetically, which increases the $^{17}\Delta$, and that from gaseous exchange with atmospheric O_2, which reduces the $^{17}\Delta$ value. In October 2013, the mixed layer was relatively deep and with high $^{17}\Delta$ values varying between 69 and 122 per meg. The $^{17}\Delta$ gradually increased with depth to a maximum of 182 per meg at 80 m, and then decreased (Fig. 3a). During months with persistent monsoon winds, highest changes in $^{17}\Delta$ and $\Delta(O_2/Ar)$ occurred in the thermocline. On August 5th the $^{17}\Delta$ maximum of 218 per meg was at 100 m. Conversely, in April the $^{17}\Delta$ variations were comparatively subtle, without a prominent sharp peak, and with values between 125 and 140 per meg in the upper 150 to 50 m depth. During the winter NEM period 17Δ was rather low at 200 m accompanied by higher $\Delta(O_2/Ar)$ in contrast to the more positive $^{17}\Delta$ recorded during the summer SWM. Below in the deeper regions, $^{17}\Delta$ remained relatively high, with increased $^{17}\Delta$ values at 1000 m in August 2014, and at 800 m in April 2015.

Moved (insertion) [9]

Moved (insertion) [10]

Moved down [11]: ¶
Our seasonal depth profiles from SEATS share some similarities with the tropical oligotrophic HOT station (Juranek and Quay, 2005), albeit with different $^{17}\Delta$ magnitudes. Notably, the $^{17}\Delta$ depth distribution pattern at SEATS was comparable to that at HOT, with a broad summer $^{17}\Delta$ peak (above 200 per meg at 80 and 100 m depth) from August 2014 comparable to that at HOT during the same month (with values above 140 per meat at 120 and 150 m depth), as well as a high peak in October 2013 (above 180 per meg at 80 m) rather similar to that at HOT during October (above 140 per meg at 100 m). In February, the $^{17}\Delta$ values were overall much lower at HOT, reaching the highest values in the deep (above 90 per meg between 150 and 200 m).

Deleted: Possibly, such trends could also be expected for SEATS, in fact our data from April 2015 appears to bear the closest resemblance to it, although a comparison of the same months would be preferrable. Lastly, we note that our maximum upper ocean $^{17}\Delta$ values in the euphotic zone at SEATS were 218 per meg at 100 m, as observed on 5th August 2014 (Fig. 3b), much higher than any previously documented upper ocean values, which typically do not exceed ~160 per meg.

Deleted: *August 2014 – summer southwest monsoon (SWM) season.*

Formatted: English (UK)

Formatted: English (UK)

Deleted: In August 2014, the $^{17}\Delta$ in the mixed layer oscillated daily between ~40−70 per meg, indicating an intermittent alternation between biological and atmospheric O_2 source (Fig. 3b). The photosynthetic activity, is expected to be minimal during this month, as supported by the low fluorescence (Fig. 4b), and may be attributed to the characteristic strong thermal stratification and nutrient depletion during summer months at SEATS (Wong et al., 2017 ... [1]

Jurikova et al., 2016) due to fractionation at equilibrium where the $\delta^{17}O$ and $\delta^{18}O$ slopes (λ) during invasion and evasion follow a slope different to that of respiration. Marine photosynthesis increases the $^{17}\Delta$ of dissolved O_2 up to its maximum value of 250 per meg (the $^{17}\Delta$ of seawater), which indicates that the dissolved O_2 is completely of photosynthetic origin, while gas exchange with atmosphere drives the $^{17}\Delta$ back towards its equilibrium value. Respiration consumes O_2, but does not affect the relative proportion of $\delta^{17}O$ and $\delta^{18}O$, and hence the $^{17}\Delta$. Respiration may, however, be traced by the $\Delta(O_2/Ar)$ since O_2 and Ar have similar physical processes, but Ar does not have any biological sources and sinks. The $^{17}\Delta$ and $\Delta(O_2/Ar)$ coupled thus serve as a powerful monitor of photosynthetic vs. atmospheric influences on dissolved O_2.

The $\Delta(O_2/Ar)$ values for the October 2013 profile are unfortunately not available and we are limited to discussing the changes in dissolved O_2 content in context of the $^{17}\Delta$ data only. In comparison to the observations from August 2014 and April 2015, interestingly, during this month we observed considerably elevated $^{17}\Delta$ in the mixed layer (90 ± 28 per meg), implying increased biological O_2 production (Table 1). High $^{17}\Delta$ values, such as the 122 per meg measured at 30 m depth seem particularly unusual, as any instantaneous increase in photosynthetic $^{17}\Delta$ signal in the mixed layer is expected to be limited due to continuous exchange with atmospheric O_2 and thus averaged against the background signal. It is also unlikely that these samples could have been affected by contamination, as any leak during the sampling or preparation would result in decreased $^{17}\Delta$ value due to influence from atmospheric O_2. A likely explanation for the observed high $^{17}\Delta$ would be the rather short O_2 production time (<1 day) against the relatively very long residence time of O_2 in the mixed layer (16 days; see Section 2.2.), suggesting a sustained accumulation of biologically produced O_2. The timing of the high $^{17}\Delta$ values in the mixed layer (Fig. 4a) also coincides with the overall highest observed fluorescence in this study (Fig. 3a). The Chl−a maximum was situated below the mixed layer in the thermocline where we also recorded a $^{17}\Delta$ peak. The high mixed layer values therefore seem to reflect transient increase in biological O_2 due to upward flux of dissolved O_2 from the Chl−a maximum horizon. In such a case the $^{17}\Delta$ and the primary production would also integrate O_2 from below the mixed layer, and may complicate the application of the steady state model. Assuming that these values really reflect the integrated O_2 production it may suggest rather high photosynthetic activity for an inter-monsoon period, probably enhanced by the onset of cooler temperatures after the summer.

The average mixed layer $^{17}\Delta$ and $\Delta(O_2/Ar)$ on August 5th and 6th 2014 as well as on April 24th 2015, were, within the variations, indistinguishable from each other (~55 per meg and ~−0.3 %; Table 1). The $^{17}\Delta$ values reflect the presence of biological O_2, while the near-equilibrium $\Delta(O_2/Ar)$ indicate gas exchange, suggesting an intermittent alternation between biological and atmospheric O_2 source (Fig. 4b). During the summer months, the photosynthetic activity at SEATS is expected to be minimal. This may be attributed to the characteristic strong thermal stratification and nutrient depletion (Wong et al., 2017b), as supported by the measured low fluorescence in August 2014 (Fig. 3b), which agrees with past observations (Liu et al., 2002). Distinct $^{17}\Delta$ and $\Delta(O_2/Ar)$ values were observed on April 25th 2015 (~26 per meg and ~1.8 %; Table 1). Although the average mixed layer signal from April 24th 2015 is more similar to the values from August 2014, if the deepest mixed layer sample from 20 m depth is removed from the calculation (despite being situated well within the mixed layer) the newly obtained mixed

Moved down [12]:). The distribution and concentration of the deep chlorophyll maximum corresponds to characteristic monsoon-forced trends (Liu et al., 2002) and demonstrates the vitality of the thermocline dwelling phytoplankton and the important role of NEM winds on determining the metabolic balance of the system.

Deleted: *April 2015 – winter north east monsoon (NEM) season.* The most obvious feature of these profiles is the overall lower $^{17}\Delta$ and higher $\Delta(O_2/Ar)$ values on the 25th in contrast to the 24th of April in the upper 50 m (Fig. 3c). Close to equilibrium $^{17}\Delta$ (~20 per meg) on the second sampling day indicate increased air-sea gas exchange rates, which drive new primary production as seen by the elev... [2]

Deleted: The overall lower $^{17}\Delta$ and $\Delta(O_2/Ar)$ values in the u... [3]

Moved down [13]: may illustrate the extent of wind-induced

Deleted: ¶ ... [4]

Formatted: English (UK)

Deleted: this

Formatted: English (UK)

Deleted: other seasonal profiles

Deleted: one shows an overall

Formatted: English (UK)

Deleted: ,

Deleted: . Values above 120 per meg

Deleted: and 50

Deleted: of

Formatted: English (UK)

Deleted: also

Formatted: English (UK)

Deleted: signal

Deleted: very

Formatted: English (UK)

Formatted: English (UK)

Deleted: 3a

Deleted: 4a), although the

Deleted: and does not fully concur

Deleted: depth with

Formatted: English (UK)

Deleted: Potentially, part of the $^{17}\Delta$ signal may also

Deleted: a

Deleted: (Fig. 4d).

Formatted: English (UK)

Deleted: Nonetheless, if the observed

Deleted: this would point towards higher production rates d... [5]

Deleted: periods than previously thought (Wong et al., 2007).

layer $\Delta(O_2/Ar)$ agree well with the data from April 25th 2015 (1.5 ± 0.2 %; although the $^{17}\Delta$ remain unaffected 46 ± 7). Close to equilibrium $^{17}\Delta$ on the following sampling day indicate increased air-sea gas exchange rates, which drive new primary production as evidenced by the elevated $\Delta(O_2/Ar)$ in the mixed layer (Fig. 4c) and also by the intensified fluorescence (Fig. 3c) and dissolved oxygen (Fig. 3d). The distribution and concentration of the deep chlorophyll maximum corresponds to characteristic monsoon-forced trends (Liu et al., 2002) and demonstrates the vitality of the thermocline dwelling phytoplankton and the important role of NEM winds on determining the metabolic balance of the system. The overall lower $^{17}\Delta$ and $\Delta(O_2/Ar)$ values in the upper water column observed in April 2015 when compared to August 2014 (Fig. 4) may illustrate the extent of wind-induced vertical mixing, which could be sufficient to reach the upper limit of the nutricline (e.g. Ning et al., 2004; Tseng et al., 2005) and supply nutrients to the phytoplankton community. Alternatively, between February and April monsoon winds tend to carry minerals and iron rich dust particles from the deserts in Central Asia to the northern SCS and SEATS (Lin et al., 2007; Duce et al., 1991; Fung et al., 2000), which loading could fuel the enhanced biological production. These profiles thus serve as a good example of the local ecosystem interactions and underscore the close dependence of the phytoplankton communities on the NEM forcing.

Moved (insertion) [12]

Moved (insertion) [13]

4.2 Primary production rates in South China Sea

Primary production, the synthesis of organic compounds from carbon-containing species is of critical importance to biogeochemical cycling of carbon and oxygen that sustains the marine ecosystem. In a steady-state system we may distinguish gross (GP) and net production (NP), where the former represents the total C fixed by primary producers and the latter the C available to the heterotrophic community. The NP thus amounts to the difference between the GP and community respiration. NP is positive when GP exceeds respiration and the ecosystem exports or stores organic C, while negative values result when respiration exceeds GP and the ecosystem respires more organic C than was able to produce. These terms are of fundamental interest to ocean studies. However, their quantification is not straightforward, and thus far only limited information is available globally and especially from SEATS and the SCS.

Our production rates are summarized in Table 1, derived from δ-values of dissolved oxygen using a steady-state mixed layer oxygen budget model that allows for determining integrated productivity in the mixed layer over the residence time of O_2 (as detailed in Section 2.2). We note that these estimates, however, do not account for complex physical processes (vertical mixing, lateral advection) and non-steady state effects on the mass balance. Furthermore, as discussed in Section 2.2. the choice of parametrisation method and approach for calculating gas exchange rates introduces considerable uncertainties and merits a careful consideration. The definition of the mixed layer depth is also highly relevant, although as shown both the temperature-based and dissolved O_2-based definition resulted in similar depths in this study. By far and large, we found that the greatest measurable uncertainties resulted from variations in $\delta^{17}O$, $\delta^{18}O$ and $\Delta(O_2/Ar)$ between samples collected from a vertical profile through the mixed layer, reported as the standard deviation of the mean composition of dissolved O_2 in the mixed layer, and which are considered for calculating our NP and GP rates.

Deleted: find minimal changes

Deleted: the

We found comparable production rates on the two consecutive sampling days in August 2014, with mean GP about ~1500 mg C m^{-2} d^{-1}, and low negative NP rates averaging −13 mg C m^{-2} d^{-1}. These rates indicate that the system metabolism is net heterotrophic, but within the observed variations (Table 1), probably close to being in net balance. Such values likely prevail during the summer SWM season, as with the exception of sporadic typhoon events, the environmental conditions can be expected to remain rather stable and the water column strongly stratified. The production was also within the errors comparable on April 5th 2015, yielding GP of about ~2000 mg C m^{-2} and NP of ~−40 mg C m^{-2} d^{-1}. On the second sampling day, April 6th, the GP was considerably lower of ~600 mg C m^{-2} d^{-1} and NP higher and positive of ~140 mg C m^{-2} d^{-1}. This points towards a more dynamic system, likely influenced by the NEM forcing, which shifts the metabolic balance of the system to net autotrophy, due to cooler temperatures and wind-induced mixing. Highest GP estimates were obtained in October 2013 of 6600 mg C m^{-2} d^{-1}, which is rather surprising since during inter-monsoon periods phytoplankton production is expected to be limited. The origin of the high GP rates in October 2013 appears related to the deep mixed layer with elevated $^{17}\Delta$ values (122 per meg) measured at 30 m, driven by O_2 contribution from the photic layer. These estimates, however, should not be taken at a face value as diapycnal mixing across the base of the mixed layer, and/or heterogenous distribution of phytoplankton in the water column and potential in situ production at depth cannot be ruled out in which case the steady state no longer applies.

It is to be stressed that our estimates represent the mixed layer production rates (rather than total water column rates). During our sampling campaigns at SEATS, the euphotic zone was persistently deeper than the mixed layer (Table 1, Fig. 3). This may lead to underestimation of the true mixed layer NP values due to mixing or entrainment of low-O_2 waters into the mixed layer, and conversely overestimation of the true mixed layer GP values due to mixing or entrainment of high-$^{17}\Delta$ waters into the mixed layer, since the share of the production that takes place within the euphotic zone below the mixed layer cannot be accounted for by the present model. Nonetheless, it is likely that if the respiration exceeds gross production in the mixed layer, and hence the NP is negative, the overall NP in the euphotic zone will also be negative, since deeper regions tend to have higher respiration rates. Thus, production estimates from paired $^{17}\Delta$ and $\Delta(O_2/Ar)$ profiles are still useful for indicating trends in ecosystem metabolism, even on instances when the depths of the mixed and euphotic layer differ. Our findings indicate that over the year respiration is close to GP and potentially even exceeds GP, but with the frequency as well as intensity of the NEM forcing likely playing a critical role in determining the overall metabolic balance of the ecosystem. Hence, production during winters with cooler temperatures and windy days may play a decisive role determining the amount of organic C fixed. Weakening of the East Asian Monsoon by anthropogenically induced global warming (e.g. Hsu and Chen, 2002; Xu et al., 2006) is, however, likely to limit vertical transport and nutrient supply to the phytoplankton. It is to be seen to what extent this will affect the primary production and overall C balance at SEATS and SCS.

Available data based on ^{14}C observations and modelling studies suggests that primary production in the SCS falls within of range of 120–170 g C m^{-2} $year^{-1}$ (Ning et al., 2004; Chen, 2005; Liu et al., 2002). These values reflect the net, euphotic-zone

Deleted: 1.8 g
Deleted: 0.02 g
Deleted: indicating overall
Deleted: heterotrophy, which
Deleted: prevails
Deleted: . The highly comparable daily trends suggest that the calculated rates might be a representative estimate for the summer period…
Deleted: are
Deleted: Conversely,
Deleted: more variable in
Deleted: approximately 2.3 g
Formatted: Superscript
Deleted: and NP of −0.16 g C m^{-2} d^{-1} on the first
Deleted: and 0.7 g
Deleted: 0.15 g
Deleted: on the second day, respectively
Deleted: during
Deleted: winter
Deleted: period that may shift from net heterotrophy
Deleted: 5.9 g
Deleted: (>120
Deleted: and 50 m
Deleted: Furthermore, we note
Deleted: the calculated
Deleted: should be considered as minimum production only. At
Deleted: during our sampling (
Deleted:), which
Deleted: an
Deleted: rates
Deleted: probably
Deleted: indeed compensate for
Deleted: overall annual consumption and lead to fixation
Deleted: , resulting in prolonged net heterotrophy, adversely affecting…

integrated production, making straightforward comparison to our NP data problematic. Nonetheless, to put it in context, assuming no seasonality, this translates to roughly 340 to 480 mg C m^{-2} d^{-1}, which is only slightly above our NP range (~43 ± 283 mg C m^{-2} d^{-1} and 143 ± 24 mg C m^{-2} d^{-1}, Table 1). This is a rather encouraging finding considering that the in situ triple oxygen isotope approach when compared to the in vitro technique tends to overestimate the production rates (Juranek and Quay, 2005; Quay et al., 2010; Jurikova et al., 2016), since it reflects time averaged rather than instantaneous production as in the case of the in vitro rates. The reason behind our relatively lower rates could be the fact that the estimates do not account for production throughout the entire euphotic zone, suggesting that a substantial part of productivity at SEATS takes place below the mixed layer. Our estimates, however, only offers a snapshot of primary production at SEATS. Further studies complementing our dataset at an increased temporal as well as vertical resolution are required to provide a more comprehensive picture of the biological production at SEATS, in particular in the mixed layer where we observed large variations between samples, and reduce the uncertainties observed.

Deleted: much higher than

Deleted: 160

Deleted: 152

Deleted: unexpected as

Deleted: Thus, unless PP rates in SCS have substantially declined over the past decade, or previous measurements were biased by favourable environmental conditions, it appears that our results underestimate the actual rates. This could be explained by

Deleted: However, the possibility that the rates simply reflect the natural variability of the system under seasonal and global changes, since observations of PP at SEATS and in the SCS are rather scarce, should not be excluded

4.3 Comparison to other tropical time-series

Initially launched in 1998, and becoming a part of the Joint Global Ocean Flux Study one year later (JGOFS; Shiah et al., 1999), the SEATS station has often been compared with the time series off Hawaii (the Hawaii Ocean Time-series, HOT), which together with the time series off Bermuda (the Bermuda Atlantic Time-series Study, BATS) were two key components of the former JGOFS program. In contrast to the typical features of tropical waters, characterized by minimal seasonal variations, and comparing to the low-latitude HOT station (Karl et al., 1996), the SEATS station located at an even lower latitude is characterised by a distinct phytoplankton biomass and primary production pattern (Tseng et al., 2005; Wong et al., 2007a). This distinct pattern is largely governed by the East Asian Monsoon, which brings seasonal changes that affect the oceanography and biogeochemistry of the SCS (Chao et al., 1996a; Liu et al., 2002).

Moved (insertion) [5]

Moved (insertion) [6]

Moved (insertion) [11]

Our seasonal depth profiles from SEATS share some similarities with the tropical oligotrophic HOT station (Juranek and Quay, 2005), albeit with different $^{17}\Delta$ magnitudes. Notably, the $^{17}\Delta$ depth distribution pattern at SEATS was comparable to that at HOT, with a broad summer $^{17}\Delta$ peak (above 200 per meg at 80 and 100 m depth) from August 2014 comparable to that at HOT during the same month (with values above 140 per meat at 120 and 150 m depth), as well as a high peak in October 2013 (above 180 per meg at 80 m) rather similar to that at HOT during October (above 140 per meg at 100 m). In February, the $^{17}\Delta$ values were overall much lower at HOT, reaching the highest values in the deep (above 90 per meg between 150 and 200 m). Possibly, such trends could also be expected for SEATS; in fact our data from April 2015 appears to bear a close resemblance to it, although a comparison of the same months would be preferrable. Our maximum $^{17}\Delta$ values within the euphotic zone at SEATS (218 per meg at 100 m observed on 5th August 2014, Fig. 3b) are, however, to our knowledge much higher than any previously documented upper ocean values (at HOT or elsewhere), which typically do not exceed ~160 per meg.

Obviating the estimates from October 2013, our GP and NP rates are comparable to those based on δ-values from HOT, where seasonal variation in GP and NP were in the range of 800–1470 mg C m^{-2} d^{-1} and –120 and 180 mg C m^{-2} d^{-1} (Juranek and Quay, 2005). Generally, we would, however, expect higher rates at SEATS, where both seasonal monsoon forcing and/or episodic typhoon events induce sufficient vertical mixing to bring nutrients to the mixed layer and stimulate primary production. Assuming that our rates present an underestimation of the productivity due to the relatively very shallow mixed layer, these differences could reconcile. Our observed variations in NP/GP (~–0.01 in August 2014, and between –0.02 and 0.23 in April 2015) also compare fairly well with the seasonal trends reported from HOT (between –0.13 and 0.13 during summer and winter; Juranek and Quay, 2005) with tendency toward heterotrophy in the summer and autotrophy during months. Very low NP/GP ratios were also observed from other low latitude regions such as the Equatorial Pacific (Hendricks et al., 2005; Stanley et al., 2010). This supports the general parallels in ecosystem metabolism in the oligotrophic regions, but also, given the broader variations in NP/GP ratios at SEATS, emphasizes the importance of the monsoon forcing on driving the dynamics of this system.

4.4 New insights into the $^{17}\Delta$ in deep water

The $^{17}\Delta$ has been traditionally applied for evaluating primary production in the upper ocean, and thus far only little is known on the $^{17}\Delta$ composition of the deep ocean. Due to the conservative behaviour of O_2 in a parcel of deep water where it may no longer be influenced by air–sea gas exchange or photosynthesis, the $^{17}\Delta$ could also present a valuable tracer for deep water mixing processes since any variations in $^{17}\Delta$ should principally result from mixing of waters with different $^{17}\Delta$ values. While respiration alone does not affect the tracer, the $^{17}\Delta$ may, however, behave non-conservatively and be altered by the combined effects of respiration and mixing. As shown by Nicholson et al. (2014) if two hypothetical parcels of water with very different δ-values (but same $^{17}\Delta$ values) mix; one with the starting composition of surface water and one that underwent a Rayleigh fractionation until 5% of oxygen remained, the resulting $^{17}\Delta$ values can become negative. Subsurface (~100–300 m) measurements in the equatorial Pacific indeed reported few negative values (Hendricks et al., 2005). Measurements from deeper profiles (700 m) were carried out in the Gulf of Elat and showed that the $^{17}\Delta$ below the thermocline varied considerably with seasons, a likely result of vertical as well as horizontal mixing (Wurgaft et al., 2013). In order to evaluate the behaviour of $^{17}\Delta$ in the deep water of SCS and its potential utility as a mixing tracer in an oceanographically very distinct system, we measured for the first time the $^{17}\Delta$ composition of deep O_2 profiles (down to 3500 m depth) from SEATS.

An overview of the oceanography of SCS is available in Wong et al. (2007a). The subsurface water masses in SCS consist of three main water masses; 1) the Tropical Water situated at around 150 m originating from near the international dateline at 20–30 °N in the North Pacific (Suga et al., 2003), 2) the North Pacific Intermediate Water centred around 500 m with a source in the subpolar regions in the North Pacific (You, 2003), and 3) the Deep Water below 2200 m. The Deep Water in the SCS basin is formed by Pacific water masses, which in the western Philippine Sea overflow the sill that separates it from the SCS. The characteristics of the deep water are rather uniform and similar to those in the western Philippine Sea, maintained by a

Deleted: compare reasonably well

Deleted: (between –

Deleted: and –0.02

Deleted: –

Deleted: 07 and 0.21

Deleted: trends

Deleted: (~0.06)

Deleted: in a

Deleted: 3

Deleted: ,

Deleted: ,

Deleted: can only

Deleted: . For instance, Wurgaft et al. (2013) showed

Deleted: 700 m deep

Deleted: which they related to

Deleted: .

Deleted: Sea

Deleted: novel

Deleted: ,

Deleted: 2007

mass balance between the inflowing deep water from the Phillipine Sea, upwelling and mixing with the shallower North Pacific Intermediate Water, and outflow at an intermediate depth through the Luzon Strait (Gong et al, 1992; Chao et al., 1996b; Hu et al., 2000).

Our data showed overall elevated $^{17}\Delta$ values (>140 per meg) below 200 m depth for both August 2014 and April 2015 profiles. Largest variations were found at 200 m with a decrease of 116 per meg from August 2014 to April 2015 (Fig. 6a), coinciding with changes in the temperature-salinity characteristics of the Tropical Water mass (Fig. 6b). The coeval decrease in $^{17}\Delta$ and increase in temperature-salinity at this depth illustrate the increased winter inflow of water to the SCS from Kuroshio through the Luzon Strait, or possibly also partially from the East China Sea through the Taiwan Strait (Fig. 1). This highlights the importance of NEM winds on driving the seasonal circulation inducing vertical mixing, which extends down to 400 m and leads to a full exchange of water masses during a winter (Fig. 6a). Historic records also support intrusions of North Pacific water masses to the South China Sea all year around with greatest strength in winter (Qu et al., 2000). Below, the deeper water remained relatively homogenous, and did not appear to be influenced by seasonal changes, marking the limit of the extent of monsoon-driven circulation influence on the mixing. Surprisingly, variations in $^{17}\Delta$ (around ~20 per meg) were found beneath the thermocline base, however, considering the low O_2 content at these depths, even very minor changes in O_2 may result in a large effect on the $^{17}\Delta$ signal, and thus their interpretation should be taken with caution. Although further observations from the SCS are needed for a more comprehensive picture, our first results advocate for the $^{17}\Delta$ as a valuable tracer of mixing processes, which brings new insights into some of the key aspects of our understanding of the circulation in SCS.

Deleted: show

Deleted: 5a

Deleted: 5b

Deleted: 5a

5 Conclusions

In summary, this study provides first insights into the $^{17}\Delta$ composition of dissolved O_2 at the SEATS station and within the SCS. We find the coupled $^{17}\Delta$ and $\Delta(O_2/Ar)$ approach a useful tracer, enabling us to monitor the seasonal changes in atmospheric vs. photosynthetic O_2 input in the upper part of the ocean. Our results showed that the net biological production at SEATS was negligible during most sampling days and close to net 0, however, increased when the system was more dynamic during a spring influenced by the northeast monsoon forcing. Moreover, we find the $^{17}\Delta$ of the deep water a promising tracer for physical mixing process, permitting us to evaluate the extent of the basin-wide monsoon-driven circulation in the water column and at depth, as well as revisit the deep mixing processes. Although further work is required before the deep $^{17}\Delta$ may be confidently applied as a tracer of water mass mixing, our study shows that it could bring new perspectives on the renewal rate of deep water, at least within the South China Sea, and thus further deep $^{17}\Delta$ measurements within the region but also globally would be desirable. Likewise, future studies considering increased spatio-temporal resolution of upper water $^{17}\Delta$ measurements within the SCS would be beneficial for gaining a more comprehensive picture of the primary productivity dynamics in the SCS and its responses to the East Asian Monsoon and other episodic or interannual phenomena.

Deleted: show

Deleted: O_2

Deleted: is highest

Deleted: winter, closely dependent on

Deleted: , which intensity appears to dictate the sufficiency of the ecosystem to shift to net autotrophy.

Deleted: novel

Deleted: conservative

Deleted: Lastly, we would like to encourage

Deleted: , which will

Deleted: critical

Deleted: into

Deleted: monsoon

Deleted: /

Deleted: anthropogenic influences.

Data availability

The data used in this study is available in the accompanying Supplement including geochemical data (Table S1), CTD data (Table S2) and wind speed data (Table S3).

Deleted: geochemical
Deleted: are
Deleted: Supplement
Deleted: this contribution.
Deleted: are available upon request.

Acknowledgements

This work was in part supported by the Ministry of Science and Technology (MOST), Taiwan grant 108-2111-M-001-011-MY3 to Academia Sinica, and Academia Sinica Investigator Award AS-IA-109-M03. We thank Chao-Chen Lai, Hsiang-Yi Kuo, Kuo-Yuan Lee and Jen-Hua Tai for assistance during sampling and providing us shipboard data, and Hsin-Chien Liang for providing us satellite data (from the Research Center for Environmental Changes, Academia Sinica). Support from Taiwan's R/V Ocean Researcher-1 and the crew members is also gratefully acknowledged.

Deleted: a

References

Barkan E. and Luz B.: High-precision measurements of $^{17}O/^{16}O$ and $^{18}O/^{16}O$ of O_2 and O_2/Ar ratio in air. Rapid Communication in Mass Spectrometry 17, 2809–2814, https://doi.org/10.1002/rcm.1267, 2003.

Benson B. B. and Krause Jr. D. K.: The concentration and isotopic fractionation of oxygen dissolved in freshwater and seawater in equilibrium with the atmosphere. Limnology and Oceanography 29, 620–632, https://doi.org/10.4319/lo.1984.29.3.0620, 1984.

Cai W.-J. and Dai M.: Comment on ''Enhanced open ocean storage of CO_2 from shelf sea pumping''. Science 306, 1477, https://doi.org/10.1126/science.1102132, 2004.

Castro-Morales K. and Kaiser J.: Using dissolved oxygen concentrations to determine mixed layer depths in the Bellingshausen Sea. Ocean Science 8, 1–10, https://doi.org/10.5194/os-8-1-2012, 2012.

Castro-Morales K., Cassar N., Shoosmith D. R., and Kaiser J.: Biological production in the Bellingshausen Sea from oxygen-to-argon ratios and oxygen triple isotopes. Biogeosciences 10, 2273–2291, https://doi.org/10.5194/bg-10-2273-2013, 2013.

Chao S.-Y., Shaw P.-T., Wu S.S.: El Niño modulation of the South China Sea circulation. Progress in Oceanography 38, 51–93, https://doi.org/10.1016/S0079-6611(96)00010-9, 1996a.

Chao S.-Y., Shaw P.-T., Wu S.S.: Deep water ventilation in the South China Sea. Deep-Sea Research I 43, 445–466, https://doi.org/10.1016/0967-0637(96)00025-8, 1996b.

Chen C.-C., Shiah F.-K., Chung S.-W., Liu K.-K.: Winter phytoplankton blooms in the shallow mixed layer of the South China Sea enahnced by upwelling. Journal of Marine Systems 59, 97–110, https://doi.org/10.1016/j.jmarsys.2005.09.002, 2006.

Chen C.-T. A., Liu K.-K.., Macdonald R.: Continental margin exchanges, in Ocean Biogeochemistry: The Role of the Ocean Carbon Cycle in Global Change. Edited by M. J. R. Fasham, Springer, New York, 53–98, https://doi.org/10.1007/978-3-642-55844-3_4, 2003.

Chen, Y. L.: Spatial and seasonal variations of nitrate-based new production and primary production in the South China Sea. Deep-Sea Research I 52, 319–340, https://doi.org/10.1016/j.dsr.2004.11.001, 2005.

Carr M.-E., et al.: A comparison of global estimates of marine primary production from ocean color. Deep-Sea Research II 53, 741–770, https://doi.org/10.1016/j.dsr2.2006.01.028, 2006.

Duce R.A., et al. The atmospheric input of trace species to the world ocean. Global Biogeochemical Cycles 5, 193–259, https://doi.org/10.1029/91GB01778, 1991.

DeGrandpre M.D., Olbu G.J., Beatty C.M., Hammar T.R.: Air-CO_2 fluxes on the US Middle Atlantic Bight. Deep Sea Research Part II: Topical Studies in Oceanography 49, 4355–4367, https://doi.org/10.1016/S0967-0645(02)00122-4, 2002.

Emerson S., Quay P. D., Stump C., Wilbur D., and Schudlich R.: Chemical tracers of productivity and respiration in the subtropical Pacific Ocean. Journal of Geophysical Research: Oceans 100, 15873–15887, https://doi.org/10.1029/95JC01333, 1995.

Frankignoulle M. and Borges A.V.: European continental shelf as a significant sink for atmospheric carbon dioxide. Global Biogeochemical Cycles 15, 569–576, https://doi.org/10.1029/2000GB001307, 2001.

Fung I.Y., Meyn S.K., Tegen I., Doney S.C., John J.G., Bishop J.K.B.: Iron supply and demand in the upper ocean. Global Biogeochemical Cycle 14, 281–296, https://doi.org/10.1029/1999GB900059, 2000.

Gong G.-C., Liu K.K., Liu C.-T., and Pai S.-C.: The chemical hydrography of the South China Sea west of Luzon and a comparison with the West Philippine Sea. TAO 3, 587-602, https://doi.org/10.3319/TAO.1992.3.4.587(O), 1992.

Gong G.-C., Chen Y.-L. L., and Liu K.-K.: Chemical hydrography and chlorophyll a distribution in the East China Sea in summer: implications in nutrient dynamics. Cont. Shelf Res. 16, 1561–1590. https://doi.org/10.1016/0278-4343(96)00005-2, 1996.

Hamme R. C., Cassar N., Lance V. P., Vaillancourt R. D., Bender M. L., Strutton P. G., Moore T. S., DeGrandpre M. D., Sabine C. L., Ho D. T., and Hargreaves B. R.: Dissolved O_2/Ar and other methods reveal rapid changes in productivity during a Lagrangian experiment in the Southern Ocean. Journal of Geophysical Research 117, C00F12, https://doi.org/10.1029/2011JC007046, 2012.

Hendricks M.B., Bender M.L., Barnett B.A.: Net and gross O_2 production in the Southern Ocean from measurements of biological O_2 saturation and its triple isotope composition. Deep Sea Research Part I: Oceanographic Research Papers 51, https://doi.org/10.1016/j.dsr.2004.06.006, 1541–1561, 2004.

Hendricks M.B., Bender M.L., Barnett B.A., Strutton P., Chavez F.P.: Triple oxygen isotope composition of dissolved O_2 in the equatorial Pacific: A tracer of mixing, production, and respiration. Journal of Geophysical Research 110, C12021, https://doi.org/10.1029/2004JC002735, 2005.

Hu J., Kawamura H., Hong H., and Qi Y.: A Review on the Currents in the South China Sea: Seasonal Circulation, South China Sea Warm Current and Kuroshio Intrusion. Journal of Oceanography 56, 607–624, https://doi.org/10.1023/A:1011117531252, 2000.

Hsu H.-H. and Chen C.-T.: Observed and projected climate change in Taiwan. Meteorology and Atmospheric Physics 79, 87–104, https://doi.org/10.1007/s703-002-8230-x, 2002.

Juranek L.W. and Quay P.D.: In vitro and in situ gross primary and net community production in the North Pacific Subtropical Gyre using labelled and natural abundance isotopes of dissolved O_2. Global Biogeochemical Cycles 19, GB30009, https://doi.org/10.1029/2004GB002384, 2005.

Juranek L. W. and Quay P. D.: Using triple isotopes of dissolved oxygen to evaluate global marine productivity. Annual Review of Marine Science 5, 503–524, https://doi.org/10.1146/annurev-marine-121211-172430, 2013.

Deleted: Ho D.T., Law C.S., Smith M.J., Schlosser P., Harvey M., and Hill P.: Measurements of air-sea gas exchange at high wind speeds in the Southern Ocean: Implications for global parametrizations. Geophysical Research Letters 33, L16611, https://doi.org/10.1029/2006GL026817, 2006.¶
¶

Juranek L. W., Quay P. D., Feely R. A., Lockwood D., Karl D. M., and Church M. J.: Biological production in the NE Pacific and its influence on air-sea CO_2 flux: Evidence from dissolved oxygen isotopes and O_2/Ar. Journal of Geophysical Research 117, C05043, https://doi.org/10.1029/2011JC007450, 2012.

Jurikova H., Guha T., Abe O., Shiah F.-K., Wang C.-H., and Liang M.-C.: Variations in triple isotope composition of dissolved oxygen and primary production in a subtropical reservoir. Biogeosciences 13, 6683–6698, https://doi.org/10.5194/bg-13-6683-2016, 2016.

Kaiser J., Reuer M. K., Barnett B., and Bender M. L.: Marine productivity estimates from O_2/Ar ratio measurements by membrane inlet mass spectrometry. Journal of Geophysical Research 32, L19605, https://doi.org/10.1029/2005GL023459, 2005.

Kaiser J.: Technical note: Consistent calculation of aquatic gross production from oxygen triple isotope measurements. Biogeosciences 8, 1793–1811, https://doi.org/10.5194/bg-8-1793-2011, 2011.

Karl D.M. and Lukas R.: The Hawaii Ocean Time-series (HOT) program: Background, rationale and field implementation. Deep Sea Research Part II: Topical Studies in Oceanography 43, 129–156, https://doi.org/10.1016/0967-0645(96)00005-7, 1996.

Lai C.-C., Wu C.-R., Chuang C.-Y., Tai J.-H., Lee K.-Y., Kuo H.-Y., and Shiah F.-K.: Phytoplankton and Bacterial Responses to Monsoon-Driven Water Masses Mixing in the Kuroshio Off the East Coast of Taiwan. Frontiers in Marine Science 8, 707807, https://doi.org/10.3389/fmars.2021.707807, 2021.

Laws E. A.: Photosynthetic quotients, new production and net community production in the open ocean. Deep-Sea Research I 38, 143– 167, https://doi.org/10.1016/0198-0149(91)90059-O, 1991.

Laws E. A., Landry M. R., Barber, R. T., Campbell L., Dickson M. L., and Marra J.: Carbon cycling in primary production bottle incubations: inferences from grazing experiments and photosynthetic studies using ^{14}C and ^{18}O in the Arabian Sea. Deep-Sea Research Part II, 47, 1339–1352, https://doi.org/10.1016/S0967-0645(99)00146-0, 2000.

Lämmerzahl P., Röckmann T., Brenninkmeijer C.A.M., Krankowsky D., Mauersberger K.: Oxygen isotope composition of stratospheric carbon dioxide. Geophysical Research Letters 29, 1582, https://doi.org/10.1029/2001GL014343, 2002.

Deleted: Res.

Li H., Wiesner M.G., Chen J., Ling Z., Zhang J., Ran L.: Long-term variation of mesopelagic biogenic flux in the central South China Sea: Impact of monsoonal seasonality and mesoscale eddy. Deep-Sea Research Part I 126, 62−72, https://doi.org/10.1016/j.dsr.2017.05.012, 2017.

Lin I.-I., Liu W.T., Wu C.-C., Wong G.T.F., Hu C., Chen Z., Liang W.-D., Yang Y., and Liu K.-K.: New evidence for enhance ocean primary production triggered by tropical cyclone. Geophysical Research Letters 30, 1718, https://doi.org/10.1029/2003GL017141, 2003.

Lin I.-I., Chen J.-P., Wong G.T.F., Huang C.-W., Lien C.-C.: Aerosol input to the South China Sea: Results from the MODerate Resolution Imaging Spectro-radiometer, the quick Scatterometer, and the Measurements of Pollution in the Troposphere Sensor. Deep-Sea Research Part II 54, 1589−1601, https://doi.org/10.1016/j.dsr2.2007.05.013, 2007.

Lin I.-I., Lien C.-C., Wu C.-R., Wong G.T.F., Huang C.-W., Chiang T.-L.: Enhanced primary prpduction in the oligotrophic South China Sea by eddy injection in spring. Geophysical Research Letters 37, L16602, https://doi.org/10.1029/2010GL043872, 2010.

Liang M.-C. and Mahata S. (2015) Oxygen anomaly in near surface carbon dioxide reveals deep stratospheric intrusion. Scientific Reports 5, 11352, https://doi.org/10.1038/srep11352, 2015.

Liang M.-C., Mahata S., Laskar A.H., Thiemens M.H., and Newman S.: Oxygen isotope anomaly in tropospheric CO_2 and implications for CO_2 residence time in the atmosphere and gross primary productivity. Scientific Reports 7, https://doi.org/10.1038/s41598-017-12774-w, 2017.

Liu K.-K., Atkinson L., Chen C.T.A., Gao S., Hall J., MacDonald R.W., McManus L.T., Quiñones R.: Exploring continental margin carbon fluxes on a global scale. EOS 81, 641–644, . https://doi.org/10.1029/EO081i052p00641-01, 2000.

Liu K.-K., Chao S.-Y., Shaw P.T., Gong G.-C., Chen C.-C., Tang T.Y.: Monsoon-forced chlorophyll distribution and primary production in the South China Sea: observations and a numerical study. Deep-Sea Research Part I 49, 1387−1412, https://doi.org/10.1016/S0967-0637(02)00035-3, 2002.

Lorenzen C.J.: Chlorophyll b in the eastern North Pacific Ocean. Deep-Sea Research 28A, 1049–1056, https://doi.org/10.1016/0198-0149(81)90017-0, 1981.

Luz B. and Barkan E.: Assessment of Oceanic Productivity with the Triple-Isotope Composition of Dissolved Oxygen. Science 288, 2028–2031, https://doi.org/ 10.1126/science.288.5473.2028, 2000.

Luz B. and Barkan E.: The isotopic ratios $^{17}O/^{16}O$ and $^{18}O/^{16}O$ in molecular oxygen and their significance in biogeochemistry. Geochimica et Cosmochimica Acta 69, 1099–1110, https://doi.org/10.1016/j.gca.2004.09.001, 2005.

Luz B., Barkan E., Bender M. L., Thiemens M. H., and Boering K. A.: Triple-isotope composition of atmospheric oxygen as a tracer of biosphere productivity. Nature 400, 547–550, https://doi.org/10.1038/22987, 1999.

Luz B., Barkan E., Sagi Y., and Yacobi Y. Z.: Evaluation of community respiratory mechanisms with oxygen isotopes: A case study in Lake Kinneret. Limnology and Oceanography 47, 33–42, https://doi.org/10.4319/lo.2002.47.1.0033, 2002.

Luz B., and Barkan E.: Proper estimation of marine gross O_2 production with $^{17}O/^{16}O$ and $^{18}O/^{16}O$ ratios of dissolved O_2. Geophysical Research Letters 38, L19606, https://doi.org/10.1029/2011GL049138, 2011.

Marra J.: Approaches to the measurement of plankton production, Phytoplankton productivity: carbon assimilation in marine and freshwater ecosystem. Edited by Willams P. J. le B., Thomas D. N., and Reynolds C. S. Cambridge, Blackwells, 78–108, https://doi.org/10.1002/9780470995204.ch4, 2002.

Nicholson D., Stanley R. H. R., and Doney S. C.: The triple oxygen isotope tracer of primary productivity in a dynamic ocean model: Triple oxygen isotopes in a global model. Global Biogeochemical Cycles, 28, 538–552. https://doi.org/10.1002/2013GB004704, 2014.

Ning X., Chai F., Xue H., Cai Y., Liu C., and Shi J.: Physical-biological oceanographic coupling influencing phytoplankton and primary production in the South China Sea. Journal of Geophysical Research 1009, C10005, https://doi.org/10.1029/2004JC002365, 2004.

Pai S. C., Gong G. C., and Liu K. K.: Determination of dissolved oxygen in seawater by direct spectrophotometry of total iodine. Marine Chemistry 41, 343–351, https://doi.org/10.1016/0304-4203(93)90266-Q, 1993.

Prokopenko M. G., Pauluis O. M., Granger J., and Yeung L. Y.: Exact evaluation of gross photosynthetic production from the oxygen triple-isotope composition of O_2: Implications for the net-to-gross primary production ratios. Geophysical Research Letters 38, L14603, https://doi.org/10.1029/2011GL047652, 2011.

Qu T., Mitsudera H., Yamagata T.: Intrusion of the North Pacific waters into the South China Sea. Journal of Geophysical Research 105, 6415–6424, https://doi.org/10.1029/1999JC900323, 2000.

Qu T., Du Y., Meyers G., Ishida A., Wang. D.: Connecting the tropical Pacific with Indian Ocean through South China Sea. Geophysical Research Letters 32, L24609, https://doi.org/10.1029/2005GL024698, 2005.

Quay P.D., Peacock C., Björkman K., Karl D.M.: Measuring primary production rates in the ocean: Enigmatic results between incubation and non-incubation methods at Station ALOHA. Global Biogeochemical Cycles 24, GB3014, https://doi.org/10.1029/2009GB003665, 2010.

Regaudie-de-Gioux A., Lasternas S., Augustí S., and Duarte C.M.: Comparing marine primary production estimates through different methods and development of conversion equations. Frontiers in Marine Science 1, 19, https://doi.org/10.3389/fmars.2014.00019, 2014.

Rehder G. and Suess E.: Methane and pCO_2 in the Kuroshio and the South China Sea during maximum summer surface temperatures. Marine Chemistry 75, 89–108, https://doi.org/10.1016/S0304-4203(01)00026-3, 2001.

Reuer M.K., Barnett B.A., Bender M.L., Falkowski P.G., Hendricks M.B.: New estimates of Southern Ocean biological production rates from O_2/Ar ratios and the triple isotope composition of O_2. Deep Sea Research I 54, 951–974, https://doi.org/10.1016/j.dsr.2007.02.007, 2007.

Sarma V. V. S. S., Abe O., Hashimoto S., Hinuma A., and Saino T.: Seasonal variations in triple oxygen isotopes and gross oxygen production in the Sagami Bay, central Japan. Limnology and Oceanography 50, 544–552, https://doi.org/10.4319/lo.2005.50.2.0544, 2005.

Seguro I., Marca A.D., Painting S.J., Shutler J., Suggett D.J., and Kaiser J.: High-resolution net and gross biological production during a Celtic Sea spring bloom. Progress in Oceanography 177, 101885, https://doi.org/10.1016/j.pocean.2017.12.00, 2019.

Schlitzer R.: Ocean Data View, https://odv.awi.de/, 2020.

Shiah F.-K., Liu K.-K., Tang T.-Y.: South East Asian Time-series Station established in South China Sea. US JGOFS Newsletter 10 , 8–9, 1999.

Stanley R. H. R., Kirkpatrick J. B., Cassar N., Barnett B. A., and Bender M. L.: Net community production and gross primary production rates in the western equatorial Pacific. Global Biogeochemical Cycles 24, GB4001, https://doi.org/10.1029/2009GB003651, 2010.

Steeman-Nielsen E.: The use of radioactive carbon (^{14}C) for measuring organic production in the sea. ICES Journal of Marine Science (Journal du Conseil) 18, 117–140, https://doi.org/10.1093/icesjms/18.2.117, 1952.

Strickland J.D.H and Parsons T.R.: A Practical Handbook of Seawater Analysis. Bulletin 167 (Second Edition) Fisheries Research Board of Canada, Ottawa, 1972.

Shang S., Zhang C., Hong H., Liu Q., Wong G.T.F., Hu C., and Huang B.: Hydrographic and biological changes in the Taiwan Strait during the 1997–1998 El Niño winter. Geophysical Research Letters 32, L11601, https://doi.org/10.1029/2005GL022578, 2005.

Suga T., Kato A., Hanawa K.: North Pacific Tropical Water: its climatology and temporal changes associated with the climate regime shift in the 1970s. Progress in Oceanography 47, 223–256, https://doi.org/10.1016/S0079-6611(00)00037-9, 2003.

Tai J.-H., Wong G.T.F., and Pan X. Upper water structure and mixed layer depth in tropical waters: The SEATS station in the northern South China Sea. Terrestrial, Atmospheric, and Oceanic sciences journal 28, 1019–1032, https://doi.org/10.3319/TAO.2017.01.09.01, 2017.

Tai J.-H., Chou W.-C., Hung C.-C., Wu K.-C., Chen Y.-H., Chen T.-Y., Gong G.-C., Shiah F.-K., and Chow C. H.: Short-term variability of biological production and CO_2 system around Dongsha Atoll of the northern South China Sea: Impact of topography-flow interation. Frontiers in Marine Sciences 7, 511, https://doi.org/10.3389/fmars.2020.00511, 2020.

Thomas H., Bozec Y., Elkalay K., de Baar H.J.W.: Enhanced Open Ocean Storage of CO_2 from Shelf Sea Pumping. Science 304, 1005–1008, https://doi.org/10.1126/science.1095491, 2004.

Tseng C.-M., Wong G.T.F., Lin I.-I., Wu C.-R., and Liu K.-K.: A unique seasonal pattern in phytoplankton biomass in low-latitude waters in the South China Sea. Geophysical Research Letters 32, L08608, https://doi.org/10.1029/2004GL022111, 2005.

Tseng C.-M., Wong G.T.F., Chou W.-C., Lee B.-S., Sheu D.-D., Liu K.-K.: Temporal variations in the carbonate system in the upper layer at the SEATS. Deep-Sea Research II 54, 1448–1468, https://doi.org/10.1016/j.dsr2.2007.05.003, 2007.

Tseng C.-M., Liu K.-K., Wang L.-W., Gong G.-C.: Anomalous hydrographic and biological conditions in the northern South China Sea during the 1997-1998 El Niño and comparisons with the equatorial Pacific. Deep-Sea Research I 56, 2129–2143, https://doi.org/10.1016/j.dsr.2009.09.004, 2009.

Tsunogai S., Watanabe S., and Sato T.: Is there a "continental shelf pump" for the absorption of atmospheric CO_2? Tellus 51, 701−712, https://doi.org/10.1034/j.1600-0889.1999.t01-2-00010.x, 1999.

Wang S.-L., Chen C.-T.A., Hong G.-H., and Chung C.-S.: Carbon dioxide related parameters in the East China Sea. Continental Shelf Research 2000, 525–544, https://doi.org/10.1016/S0278-4343(99)00084-9, 2000.

Wanninkhof R., Asher W. E., Ho D. T., Sweeney C., and McGillis W. R.: Advances in quantifying air-sea gas exchange and environmental forcing. Annual Review of Marine Science 1, 213–244, https://doi.org/10.1146/annurev.marine.010908.163742, 2009.

Wong G.T.F., Ku T.-L., Mulholland M., Tseng C.M., and Wang D.-P.: The SouthEast Asian Time-series Study (SEATS) and the biogeochemistry of the South China Sea – An overview. Deep-Sea Research Part II 54, 1434−1447, https://doi.org/10.1016/j.dsr2.2007.05.012, 2007a.

Wong G.T.F., Tseng C.-M., Wen L.-S., and Chung S.-W.: Nutrient dynamics and N-anomaly at the SEATS station. Deep-Sea Research Part II 54, 1528–1545, https://doi.org/10.1016/j.dsr2.2007.05.011, 2007b.

Wurgaft E., Shamir O., Barkan E., Paldor N., and Luz B.: Mixing processes in the deep water of the Gulf of Elat (Aqaba): evidence from measurements and modelling of the triple isotopic composition of dissolved oxygen. Limnology and Oceanography 58, 1373−1386, https://doi.org/10.4319/lo.2013.58.4.1373, 2013.

Xu M., Chang C.-P., Fu C., Qi Y., Robock A., Robinson D., and Zhang H.-M.: Steady decline of east Asian monsoon winds, 1969–2000: Evidence from direct ground measurements of wind speed. Journal of Geophysical Research 111, D24111, https://doi.org/10.1029/2006JD00733, 2006.

Yool A. and Fasham M.J.R.: An examination of the "Continental shelf pump" in an open ocean general circulation model. Global Biogeochemical Cycles 15, 831–844, https://doi.org/10.1029/2000GB001359, 2001.

Deleted: 2007

You Y.: The pathway and circulation of North Pacific Intermediate Water. Geophysical Research Letters 30, 2291, https://doi.org/10.1029/2003GL018561, 2003.

Zhai W., Dai M., Cai W.-J., Wang Y., Hong H.: The partial pressure of carbon dioxide and air-sea fluxes in the northern South China Sea in spring, summer and autumn. Marine Chemistry 96, 87–97, https://doi.org/10.1016/j.marchem.2004.12.002, 2005.

Zhou W. and Chan J. C. L.: ENSO and the South China Sea summer monsoon onset. International Journal of Climatology 27, 157–167, https://doi.org/10.1002/joc.1380, 2007.

Deleted: Page Break

Date	PLD[a] (m)	MLD[b] (m)	MLD[b] (m)	C_o (mmol m^{-3})	K_{avg} (m d^{-1})	K_{wgh} (m d^{-1})	$\Delta(O_2/Ar)$ (%)	$^{17}\Delta$ (per meg)	NP	GP	NCP / GCP
Oct. 16th, 2013	81	49	48	201.29	4.0	6.4		90 ± 28		6660 ± 2930	
Aug. 5th, 2014	77	25	20	198.04	4.7	3.2	−0.3 ± 0.5	59 ± 9	−18 ± 27	1620 ± 170	−0.01
Aug. 6th, 2014	79	34	32	198.04	4.7	3.2	−0.2 ± 0.2	54 ± 18	−8 ± 13	1400 ± 530	−0.01
Apr. 24th, 2015	101	28	27	204.63	5.7	4.7	−0.5 ± 3.5	52 ± 11	−43 ± 283	2010 ± 720	−0.02
Apr. 25th, 2015	101	26	25	204.63	5.7	4.7	1.8 ± 0.3	26 ± 5	143 ± 24	620 ± 250	0.23

[a]Photic layer depth. [b]Temperature-based mixed layer depth. [c]O_2-based mixed layer depth.

185 **Table 1: Mixed-layer dissolved oxygen composition, and estimated seasonal primary production rates at the SouthEast Asian Time-series Study (station 55, "SEATS") in the South China Sea (SCS) for October 2013, August 2014 and April 2015. Both, NP and GP are in mg C m^{-2} d^{-1}, and were calculated using the O_2-based mixed layer depth and weighted gas exchange rate (K_{wgh}). The GP and NP uncertainities are based on $\Delta(O_2/Ar)$, $\delta^{17}O$ and $\delta^{18}O$ variations between dissolved O_2 samples collected from a vertical profile through the mixed layer (1σ of the mean, n = 3 for each sampling day).**

Inserted Cells ... [7]
Deleted: K from U¶
Formatted ... [8]
Formatted ... [6]
Inserted Cells ... [10]
Formatted ... [11]
Formatted ... [9]
Formatted ... [12]
Deleted: 3.1
Formatted ... [14]
Deleted: –
Deleted: 123
Deleted: –
Deleted: 5895
Formatted ... [17]
Formatted ... [18]
Formatted ... [19]
Deleted: –
Formatted ... [20]
Inserted Cells ... [21]
Formatted ... [13]
Formatted ... [15]
Formatted ... [16]
Formatted ... [22]
Deleted: 31
Formatted ... [23]
Inserted Cells ... [24]
Formatted ... [25]
Deleted: 6
Deleted: 29
Formatted ... [28]
Deleted: 1830
Formatted ... [29]
Deleted: 02
Formatted ... [26]
Formatted ... [27]
Formatted ... [30]
Formatted ... [31]
Deleted: 31
Formatted ... [32]
Formatted ... [33]
Deleted: 6
Formatted ... [34]
Deleted: 57
Formatted ... [35]
Deleted: 15
Formatted ... [36]
Deleted: 1761
Formatted ... [37]
Formatted ... [38]
Deleted: 23
Formatted ... [39]
Formatted ... [40]
Deleted: 6

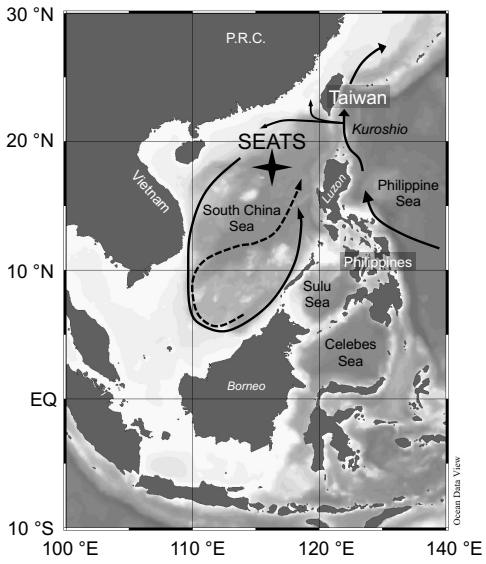

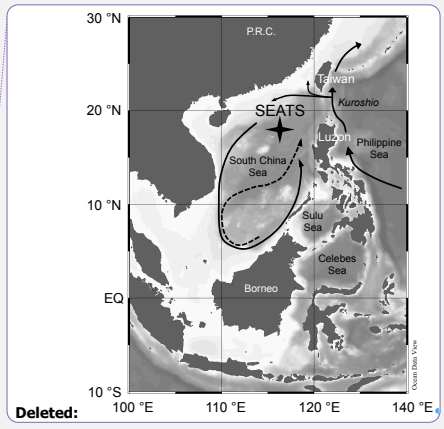

Deleted:

Figure 1: Bathymetric map of South China Sea (SCS) and surrounding areas with position of The SouthEast Asian Time-series Study (station 55, "SEATS") indicated. Arrows in SCS indicate the circulation patterns – solid line shows the basin-wide cyclonic gyre during winter, dashed line represents the eastward jet off the Vietnam coast and the anticyclonic gyre over the southern half of SCS throughout the summer. Map was created using Ocean Data View (https://odv.awi.de/; Schlitzer, 2020).

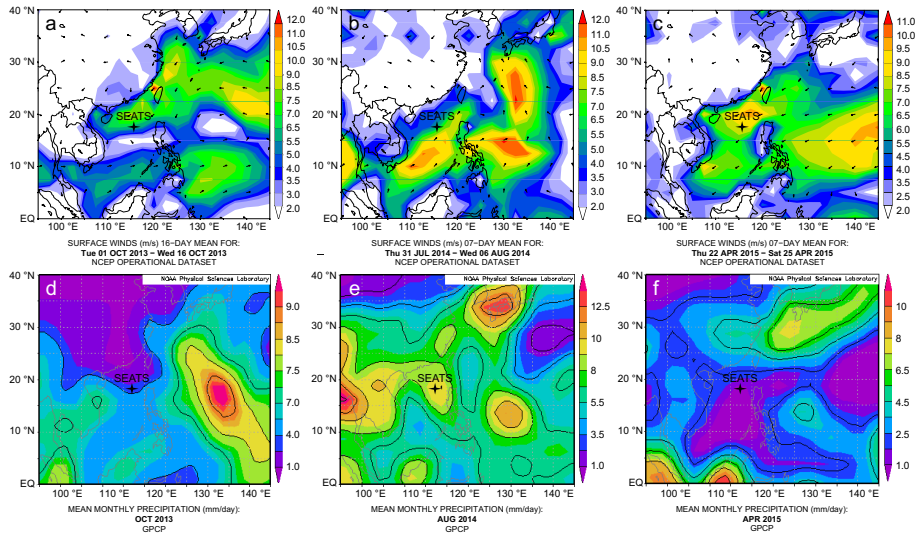

Figure 2: Upper panels – surface vector wind maps indicating the monsoon seasons: a) inter-monsoon period in October 2013; b) southwest summer monsoon in August 2014; c) northeast winter monsoon in April 2015. Lower panels – mean monthly precipitation: d) in October 2013; e) in August 2014; c) and in April 2015. Maps of vector winds distributions were obtained from the NOAA – Atmospheric Variables Plotting Page using the NCEP daily analysis data (https://www.esrl.noaa.gov/psd/data/histdata/). Maps of precipitation were obtained from NOAA's GPCP Version 2.3 Combined Precipitation Data Set (https://psl.noaa.gov/data/gridded/data.gpcp.html).

Deleted:

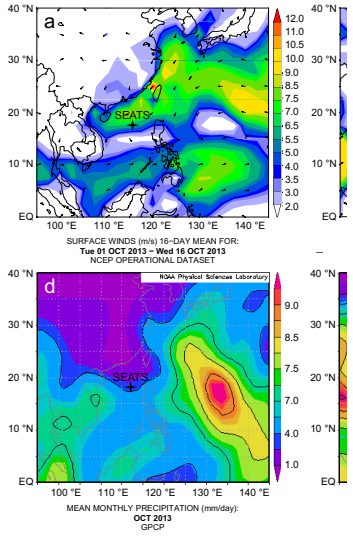

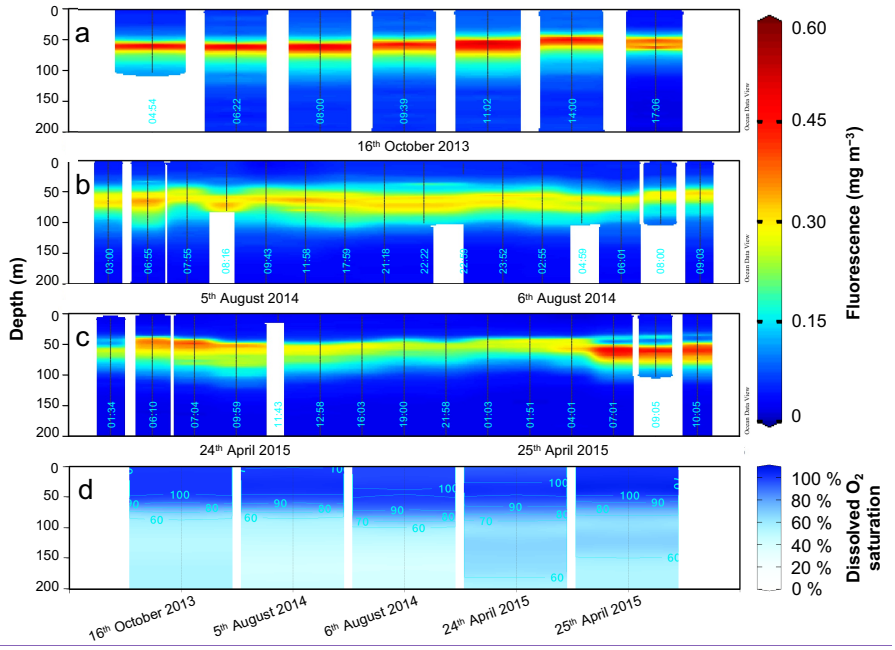

Figure 3: Fluorescence (mg m^{-3}) time-series from SEATS on: a) 16th October 2013; b) 5th–6th August 2014 and; c) 24th–25th April 2015). d) Depth profiles of dissolved O_2 saturation (%) during the different sampling days, calibrated to manual dissolved O_2 measurements. Data visualisation was done using Ocean Data View (https://odv.awi.de/; Schlitzer, 2020).

Moved (insertion) [14]

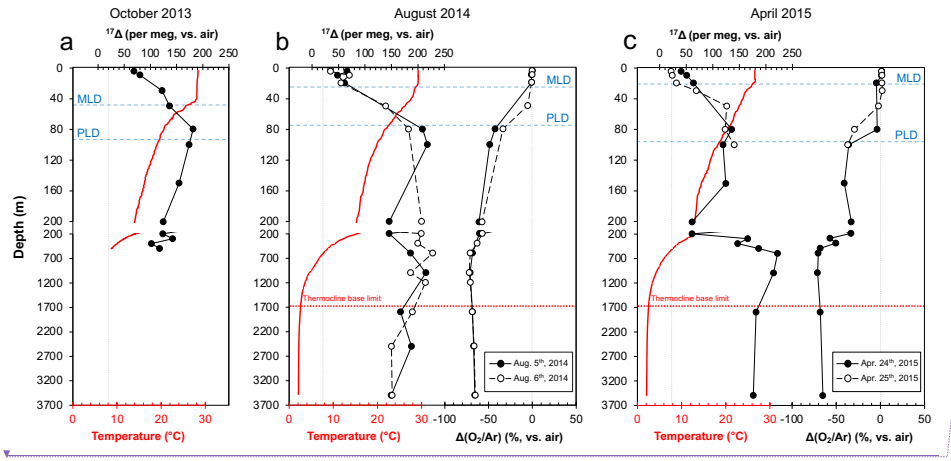

Figure 4: Depth profiles of temperature (red lines) and $^{17}\Delta$ and $\Delta(O_2/Ar)$ profiles (solid or dashed black lines) from SEATS during: a) inter-monsoon seasons; b) summer southwest (SWM); and c) winter northeast monsoon (NEM). Vertical dashed grey lines indicate the equilibrium $^{17}\Delta$ and $\Delta(O_2/Ar)$ values with atmosphere. MLD=mixed layer depth, PLD=photic layer depth.

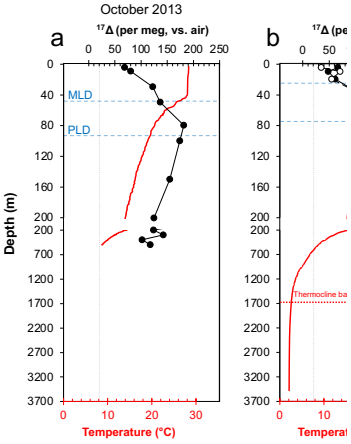

Deleted: Figure 3

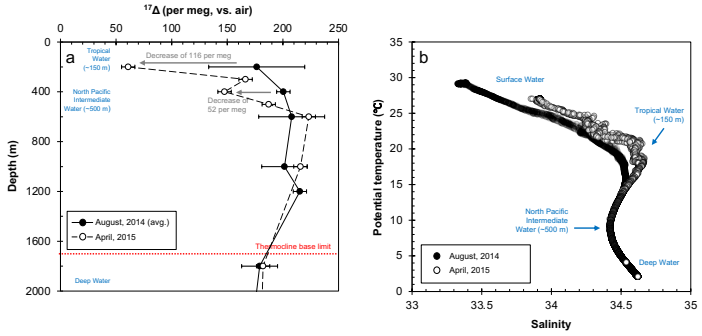

Figure 5: Deep water composition at SEATS from August 2014 to April 2015; a) $^{17}\Delta$ of dissolved O_2. Error bars indicate the standard deviation between duplicates (1σ) where available or the analytical uncertainty (6 per meg; 1σ) The $^{17}\Delta$ values from August 2014 are presented as mean of the two sampling days (5th and 6th). b) relationship between potential temperature and salinity. Salinity peak of ~34.6 (and ~20 °C) corresponds to the Tropical Water situated around 150 m, while the minimum of ~34.4 indicates the North Pacific Intermediate at around 500 m. The Deep Water below the thermocline base (~1700 m) is characterised by low temperatures ~2 °C and high salinities around ~34.6.

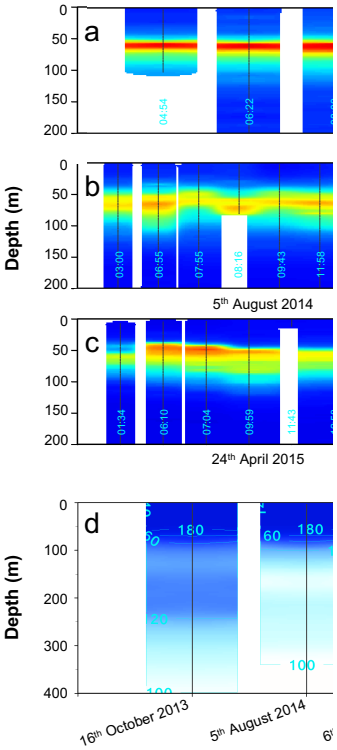

Deleted: **Figure 4: Depth profiles of fluorescence (mg m^{-3}) time-series from SEATS: a) inter-monsoon period (16th October 2013); b) summer southwest (SWM; 5th–6th August 2014); and c) winter northeast monsoon (NEM; 24th–25th April 2015); and dissolved oxygen concentration (μmol kg^{-1}) in the upper water column on the different sampling days. Maps were created**

Moved up [14]: **using Ocean Data View (https://odv.awi.de/; Schlitzer, 2020).**

Page Break

Formatted: Superscript

Formatted: Superscript

Page 9: [1] Deleted **HJ** **24/09/2021 01:52:00**

Page 10: [2] Deleted **HJ** **24/09/2021 01:52:00**

Page 10: [3] Deleted **HJ** **24/09/2021 01:52:00**

Page 10: [4] Deleted **HJ** **24/09/2021 01:52:00**

Page 10: [5] Deleted **HJ** **24/09/2021 01:52:00**

Page 26: [6] Formatted **HJ** **24/09/2021 01:52:00**

English (UK)

Page 26: [7] Inserted Cells **HJ** **24/09/2021 01:52:00**

Inserted Cells

Page 26: [8] Formatted **HJ** **24/09/2021 01:52:00**

English (UK)

Page 26: [9] Formatted **HJ** **24/09/2021 01:52:00**

English (UK)

Page 26: [10] Inserted Cells **HJ** **24/09/2021 01:52:00**

Inserted Cells

Page 26: [11] Formatted **HJ** **24/09/2021 01:52:00**

English (UK)

Page 26: [12] Formatted **HJ** **24/09/2021 01:52:00**

English (UK)

Page 26: [13] Formatted **HJ** **24/09/2021 01:52:00**

English (UK)

Page 26: [14] Formatted **HJ** **24/09/2021 01:52:00**

English (UK)

Page 26: [15] Formatted **HJ** **24/09/2021 01:52:00**

Centred

Page 26: [16] Formatted **HJ** **24/09/2021 01:52:00**

English (UK)

Page 26: [19] Formatted HJ 24/09/2021 01:52:00
English (UK)

Page 26: [20] Formatted HJ 24/09/2021 01:52:00
English (UK)

Page 26: [21] Inserted Cells HJ 24/09/2021 01:52:00
Inserted Cells

Page 26: [22] Formatted HJ 24/09/2021 01:52:00
English (UK)

Page 26: [23] Formatted HJ 24/09/2021 01:52:00
English (UK)

Page 26: [24] Inserted Cells HJ 24/09/2021 01:52:00
Inserted Cells

Page 26: [25] Formatted HJ 24/09/2021 01:52:00
English (UK)

Page 26: [26] Formatted HJ 24/09/2021 01:52:00
English (UK)

Page 26: [26] Formatted HJ 24/09/2021 01:52:00
English (UK)

Page 26: [27] Formatted HJ 24/09/2021 01:52:00
English (UK)

Page 26: [28] Formatted HJ 24/09/2021 01:52:00
English (UK)

Page 26: [29] Formatted HJ 24/09/2021 01:52:00
English (UK)

Page 26: [30] Formatted HJ 24/09/2021 01:52:00
English (UK)

Page 26: [31] Formatted HJ 24/09/2021 01:52:00
English (UK)

Page 26: [32] Formatted HJ 24/09/2021 01:52:00
English (UK)

Page 26: [33] Formatted HJ 24/09/2021 01:52:00
English (UK)

Page 26: [35] Formatted HJ 24/09/2021 01:52:00
English (UK)

Page 26: [36] Formatted HJ 24/09/2021 01:52:00
English (UK)

Page 26: [37] Formatted HJ 24/09/2021 01:52:00
English (UK)

Page 26: [38] Formatted HJ 24/09/2021 01:52:00
English (UK)

Page 26: [39] Formatted HJ 24/09/2021 01:52:00
English (UK)

Page 26: [40] Formatted HJ 24/09/2021 01:52:00
English (UK)

Page 26: [41] Formatted HJ 24/09/2021 01:52:00
English (UK)

Page 26: [42] Formatted HJ 24/09/2021 01:52:00
English (UK)

Page 26: [43] Formatted HJ 24/09/2021 01:52:00
English (UK)

Page 26: [44] Formatted HJ 24/09/2021 01:52:00
English (UK)

Page 26: [45] Formatted HJ 24/09/2021 01:52:00
English (UK)

Page 26: [46] Formatted HJ 24/09/2021 01:52:00
English (UK)

Page 26: [47] Formatted HJ 24/09/2021 01:52:00
English (UK)

Page 26: [48] Formatted HJ 24/09/2021 01:52:00
English (UK)

Page 26: [49] Formatted HJ 24/09/2021 01:52:00
English (UK)

Page 26: [50] Formatted HJ 24/09/2021 01:52:00
English (UK)

Page 26: [53] Formatted HJ 24/09/2021 01:52:00

English (UK)

Page 26: [54] Formatted HJ 24/09/2021 01:52:00

English (UK)

Page 26: [55] Formatted HJ 24/09/2021 01:52:00

English (UK)

Page 26: [56] Inserted Cells HJ 24/09/2021 01:52:00

Inserted Cells

Page 26: [57] Formatted Table HJ 24/09/2021 01:52:00

Formatted Table

Page 26: [58] Formatted HJ 24/09/2021 01:52:00

English (UK)

Page 26: [59] Formatted HJ 24/09/2021 01:52:00

English (UK)

Page 26: [59] Formatted HJ 24/09/2021 01:52:00

English (UK)

Page 26: [60] Deleted HJ 24/09/2021 01:52:00

Page 26: [60] Deleted HJ 24/09/2021 01:52:00

Page 26: [60] Deleted HJ 24/09/2021 01:52:00

Page 26: [60] Deleted HJ 24/09/2021 01:52:00

Page 26: [61] Formatted HJ 24/09/2021 01:52:00

Superscript

Page 26: [61] Formatted HJ 24/09/2021 01:52:00

Superscript

Page 26: [62] Deleted HJ 24/09/2021 01:52:00

Page 26: [62] Deleted HJ 24/09/2021 01:52:00